

Thesis for the degree of MSc in Marine Technology in the specialization of Ship  
Design

# **Global structural design of large sailing catamaran**

By

Rens Hoefs

Performed at

Dykstra Naval Architects

This thesis (MT.21/22.042.M.) is classified as confidential in accordance with the  
general conditions for projects performed by the TUDelft.

25-07-2022

## **Company supervisors**

Responsible supervisor: Mark Leslie-Miller

Daily Supervisor(s): Mark Leslie-Miller

## **Thesis exam committee**

Chair/Responsible Professor: Henk den Besten

Staff Member: Jaap Gelling

Staff Member: Austin Kana

Company Member: Mark Leslie-Miller

## **Author Details**

Studynumber: 5400651

DELFT UNIVERSITY OF TECHNOLOGY

MASTER OF MARINE TECHNOLOGY

---

Global structural design  
of  
large sailing catamaran

---

by

Rens Hoefs

In cooperation with: Dykstra Naval Architects

July 15, 2022

Supervisors: Dr. ir. J.H. Den Besten, Ir. J.L. Gelling & Ir. M. Leslie-Miller  
Institution: Delft University of Technology  
Place: Faculty of Mechanical, Marine & Material Engineering, Delft  
Project Duration: November, 2021 - July, 2022  
Document: Thesis  
Version: 1.0

# Contents

<b>1</b>	<b>Introduction</b>	<b>2</b>
1.1	Background . . . . .	2
1.2	Report outline . . . . .	2
<b>2</b>	<b>Problem definition</b>	<b>3</b>
2.1	Global structural design . . . . .	3
2.2	Research questions . . . . .	3
<b>3</b>	<b>Loads</b>	<b>4</b>
3.1	Still water loads . . . . .	5
3.1.1	First principles . . . . .	5
3.1.2	Class based guidelines . . . . .	7
3.1.3	Comparison . . . . .	8
3.2	Wave-induced loads - head seas . . . . .	9
3.2.1	First principles . . . . .	9
3.2.2	Static wave load . . . . .	9
3.2.3	Class based guidelines . . . . .	14
3.2.4	Comparison . . . . .	18
3.3	Wave-induced loads - Quartering seas . . . . .	20
3.3.1	First principles . . . . .	20
3.3.2	Class based guidelines . . . . .	21
3.3.3	Comparison . . . . .	24
3.4	Sail loads . . . . .	26
3.5	Conclusion . . . . .	26
<b>4</b>	<b>Response</b>	<b>28</b>
4.1	Head seas . . . . .	28
4.2	Quartering seas . . . . .	29
4.2.1	Analytical model . . . . .	31
4.2.2	Finite element analysis . . . . .	40
4.3	Conclusion . . . . .	48
<b>5</b>	<b>Evaluation</b>	<b>50</b>
5.1	Conclusion . . . . .	50
5.2	Discussion . . . . .	50
5.3	Recommendations . . . . .	51
<b>A</b>	<b>Derivations</b>	<b>52</b>
A.1	Timoshenko shear coefficient . . . . .	52
A.2	Shear distribution I beam . . . . .	53

# 1 | Introduction

## 1.1 Background

Currently, the largest sailing catamaran, 'Hemisphere', is 44m and has a displacement of 300t. For this research, the concept design is an aluminium catamaran of 100m with a displacement of 3000t, making this yacht a unique project in a new field. The scope of this research will be the global structure design. First, the global loads will be examined. Next, the structure will be designed and analysed to keep the responses within certain limits. Finally, the analysed responses of the structure can be used to optimise the global structural design.

### Vessel specification

Table 1.1: Dimensions of catamaran

Length overall	Loa	104.75	m
Length waterline	Lwl	99.49	m
Beam overall	Boa	32.5	m
Beam waterline float	Bwl	8.16	m
Float centerline seperation	s	23.25	m
Draught canoe	Tc	4.39	m
Displacement (DWL)	$\Delta$	3000	t
Block coefficient	$C_b$	0.41	-
Max. speed	V	20	kts

### Material properties:

Table 1.2: Material properties

Material:	Young's modulus ( $E$ ): [GPa]	Poisson ratio ( $\nu$ ):	Tensile yield stress: [MPa]	Density: [kg/m <sup>3</sup> ]
Aluminium alloy 5083-H321[3]	70	0.33	215	2660

Shear modulus:

$$G = \frac{E}{2(\nu + 1)} \quad (1.1)$$

## 1.2 Report outline

In chapter 2 the problem definition is given. This chapter also states the research questions. chapter 3 closely examines the global loads applied to the sailing catamaran. First, the still water loads are examined, then the wave-induced loads for two cases and finally, the sail loads. A method for defining the longitudinal bending moment and shear force distribution in head seas is developed. The pitch connecting moment in quartering seas is also accurately determined. The next chapter analyses the loads and their responses. An analytical method is used to define the responses. This analytical method is compared to a finite element analysis to check the accuracy of the model. When the responses of the loads are known the pitch connecting moment is found to be most dominant.

# 2 | Problem definition

## 2.1 Global structural design

An architect draws a new vessel design to a customer's demand in the superyacht industry. This new vessel should withstand all loads applied to it over its lifetime. So a naval architect has to design the global structural design within the available space for the structural elements. To start the design process of this global structural design, the global loads applied to a vessel should be known. Classification societies have made guidelines which prescribe the loads a specific type of vessel needs to withstand. However, the classification societies determine the magnitude of these loads based on data of predecessors of similar types of vessels. This is great for vessels similar to previously built vessels as it simplifies the process. However, for progressive vessels or vessels of a different scale, this deterministic approach could result in very conservative or underestimating load cases due to extrapolating. Determining these loads with a more physical approach, using first principles, gives insight into how (in)correct the load cases by class societies are. Once the load cases are determined, this needs to translate into the response of the global structural design. For a catamaran, the transverse structure is of great importance. A beam element idealisation of this transverse structure could simplify and speed up the response analysis. This is very useful in the concept phase of the global structural design, as the consequences of making adjustments to the overall design if required are still relatively small. To improve the global structural design of a catamaran in the concept design phase, this research will focus on answering the research question listed in the next section.

## 2.2 Research questions

**How valuable is an analytical method in the concept design phase to derive strength and stiffness criteria for structural members based on the global loads acting on a large sailing catamaran?**

- Which global loads are dominant on large sailing catamarans?
  - Which global loads are acting on large sailing catamarans?
    - \* Which global loads are acting on large non-sailing catamarans
    - \* Which additional loads are created by the sails and the rigging.
- How can the currently used global structure analysis methods for monohulls be adapted for catamarans?
  - Which methods for processing the global loads are used for sailing monohulls?
  - Which methods for processing the global loads are currently used for non-sailing catamarans?
- How valuable is a beam element idealisation for analysing the global response on a sailing catamaran?
  - How can the conceptual design be idealised for analysis?

# 3 | Loads

This chapter takes a closer look at the global loads applied to the sailing catamaran. To be able to continue in the design process once the first dimensions are decided, it is essential to have actual strength and stiffness data. With this data, the actual hull structure can be designed sufficiently strong and stiff. To get the strength and stiffness data, first, the applied loads acting on the vessel are determined. This research is limited to the global structural design, so only the global loads are considered in this chapter. The total global load acting on a sailing vessel results from the summation of the individual loads shown below. The wave-induced loads are analysed for head seas and quartering seas as these are the most critical conditions for the longitudinal and transverse structure, respectively.

1. Still water loads
2. Wave-induced loads
  - Head seas
  - Quartering seas
3. Rigging/sailing loads

These global loads result in various forces and moments. Not all forces and moments are equally important. In large monohull design, the longitudinal strength is of importance; for multi-hull vessels, the transverse strength is just as important[8]. The forces and moments that are of importance for catamaran designs are shown in Figure 3.1 and given below:

- $M_x$  Moment around x (transverse bending)
- $M_y$  Moment around y (longitudinal bending )
- $M_z$  Moment around z (prying)
- $M_p$  Pitch connecting torsional moment
- $Q_l$  Vertical shear force on longitudinal hull girder
- $Q_t$  Vertical shear force on the transverse structure

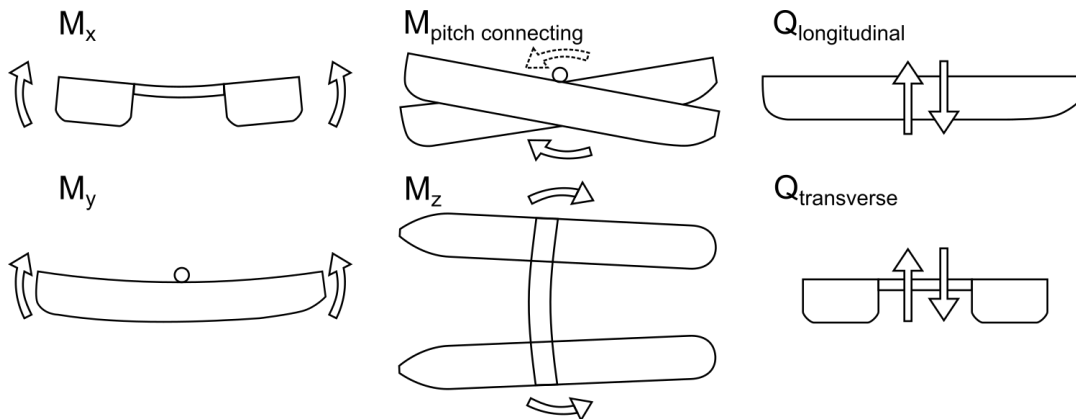


Figure 3.1: Overview of crucial moments and (shear)forces for catamaran design, where the arrows indicate the positive direction of the respective moment or shear force

These moments and forces result from different laws of physics and can be computed according to these laws, called the first principles. However, these first principles become very computationally expensive to solve for some loads. This is due to the statistical estimation of sea wave properties and the resulting forces. For this reason, classification societies have guidelines to determine the moments and forces resulting from the most critical load cases. The results from the following classification societies are analyzed: American Bureau of Shipping (ABS), Bureau Veritas (BV), Det Norske Veritas (DNV) and Lloyd's Register (LR). In addition, the guidelines by the International Organization for Standardization (ISO) are also analysed. In this chapter, the different load cases are inspected individually and it is shown in what forces and moments they result. For each load, the first principles are reviewed, which are then compared to the classification rules.

## 3.1 Still water loads

The still water loads are a result of the hydrostatic pressure in flat water on the hull and the gravitational force on the mass distribution of the vessel. The buoyancy force and the gravitational force are equal in size and counteract each other, which makes the vessel float. However, these forces are not acting in the same places, resulting in internal force and moment distributions. For monohull design, the still water load results in a longitudinal bending moment,  $M_y$ , and a longitudinal shear force distribution,  $Q_l$ , see Figure 3.1. For a multihull design, the still water load can also result in a transverse bending moment,  $M_x$ , and a transverse shear force  $Q_t$ [8] [13].

### 3.1.1 First principles

The loads can be determined with Archimedes' principle, which states that the net force on the submerged body is directed vertically and equal to the weight of the liquid that is displaced by the body. The displaced volume is a function of the weight of the vessel. The weight distribution of a vessel results in a total weight and a centre of gravity, which results in an equilibrium position of the structure. In this equilibrium position, the distributed weight of the structure and the displaced fluid by the submerged volume balance each other out. This results in hydrostatic loads. Because the catamaran is assumed symmetrical, the torsional moment  $M_p$  can be neglected for this load case. Asymmetrical loading and/or placement of tanks could result in these torsional moments. In that case, an additional load case for asymmetrical loading could be implemented.

#### Method

For defining the moments and forces, both hulls will be modelled as beams. Each beam has an upward force distribution as a result of the displacement of water, buoyancy, and a downward-facing force distribution as a result of gravitational forces on the mass. The cross deck can also be assumed as one or multiple beams with a force distribution for the mass. The buoyancy distribution together with the mass distribution results in a net load. By integrating this net load the shear force is determined. Integrating the shear force results in the bending moment.

When the exact hull shape is known more exact results can be acquired because the buoyancy distribution can be accurately determined. Commercial software is available which can easily determine the cross-sectional areas for a certain hull shape. The software places the vessel in the water on the design waterline. The cross-sectional areas of the vessel, below the waterline, can now easily be computed together with the required centre of gravity. When the design waterline is known this can also be done by hand. These sectional areas are used to determine the buoyancy distribution.

#### Result

To determine the still water loads of the subjected vessel, the hull shape is loaded into Autohydro software by Autoship. The software determines the cross-sectional areas and the centre of gravity for the ship when it is placed on the design waterline, see Figure 3.2.

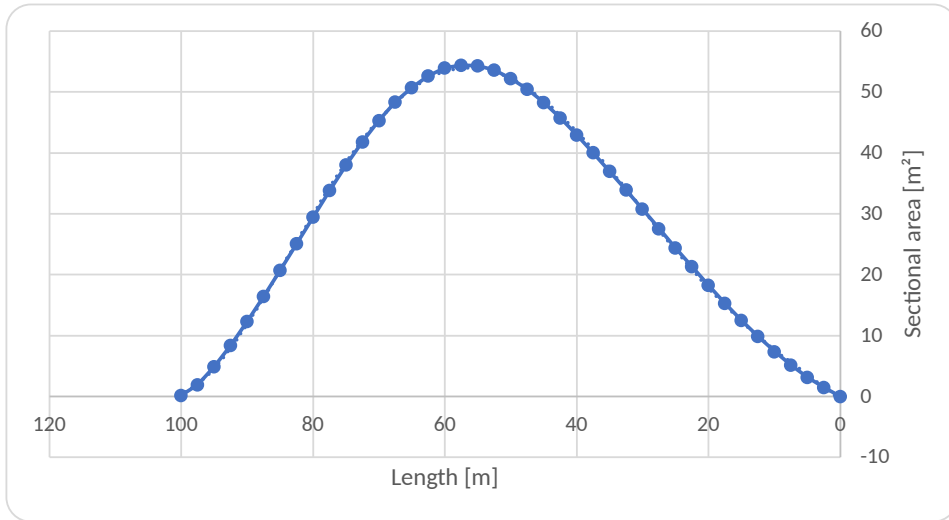


Figure 3.2: The buoyancy distribution of the vessel placed on the design waterline.

A simplified mass distribution has been assumed, see Figure 3.3. The three free-standing masts have an assumed weight of 30t each. Furthermore, the weight is divided into three equal parts, the two hulls and the cross deck are assumed equal in weight. The mass of the cross structure is constant over the distance of the cross structure. The mass of the hulls is assumed a second-order polynomial. The centre of gravity should be equal to the CoG determined by placing the vessel on the design waterline. This shaped the polynomial which resulted in the weight distribution shown in Figure 3.3.

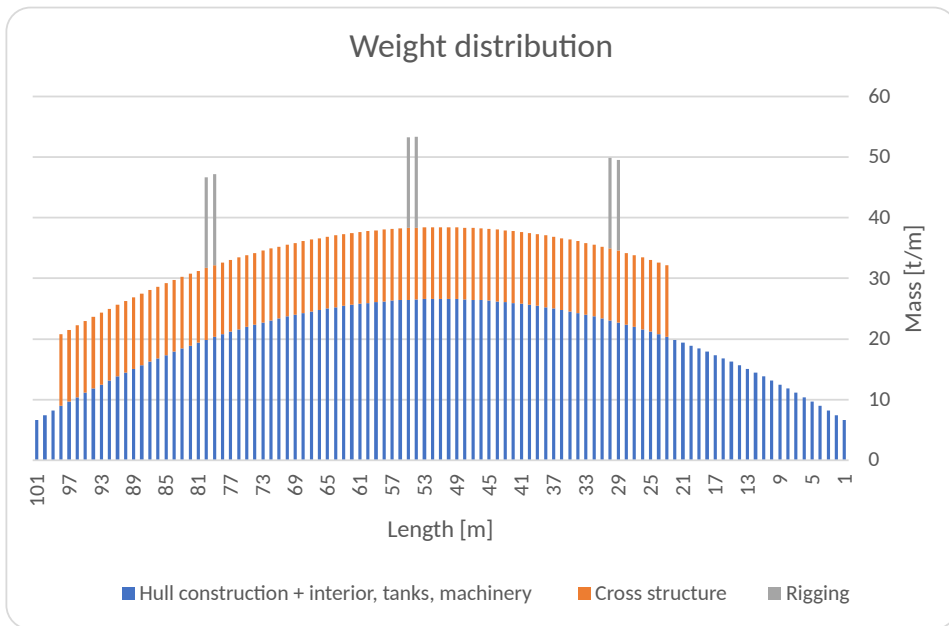


Figure 3.3: The estimated weight distribution of sailing catamaran

This weight distribution together with the cross-sectional area results in a net load over the length. Integrating this net load over the length results in the shear force distribution. Integrating the shear force results in the bending moment distribution. The still water shear force distribution is shown in Figure 3.4a and the bending moment distribution in Figure 3.4b. The shear force and bending moment at both ends should be equal to zero. Which is a good check to see whether the estimated weight distribution has the right COG and size. As can be seen in Figure 3.4b, the subject vessel will have a positive (hogging) bending moment in still water, see Figure 3.1 for the determination of positive directions.

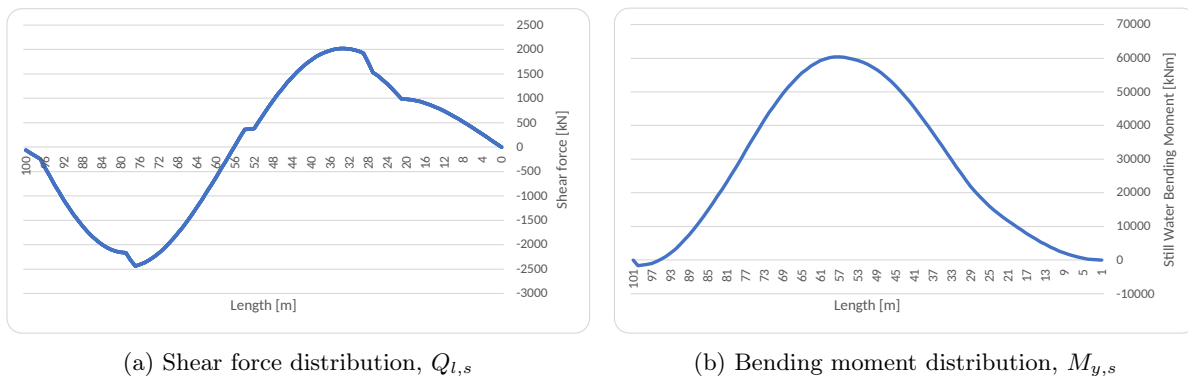


Figure 3.4: Still water load case result

### 3.1.2 Class based guidelines

The classification societies expect the still water load to be determined according to the first principles, with the method explained in subsection 3.1.1. The mentioned software can be used to ease this process. The classification societies do however demand different still water moments and forces from varying loading conditions. Some classification societies provide methods to estimate the still water loads early on in the design process. ABS, Lloyd's Register and ISO do not provide any additional methods, so are not mentioned below.

#### Bureau Veritas

BV requires the longitudinal distribution of still water bending moments and shear forces for two loading conditions, 100% (full) capacity and 10% (light) capacity. If the information required for the full still water load calculation is not available, the still water bending moment and shear forces may be taken from Equation 3.1 as a guideline for preliminary assessment only. These values are accepted during the concept design phase. BV assumes that the vessel is in hogging conditions for this preliminary assessment. For multihull designs, no transverse bending moments or shear forces are considered. The preliminary rules Figure 3.3 for determining the longitudinal bending moment and shear force distribution are given below:

$$M_{y,SW,H} = 0,8M_{y,w} \quad Q_{l,SW} = 0,8Q_{l,w} \quad (3.1)$$

[4]

Where:

- $M_{y,w}$  : Wave induced moment around Y in head seas, see Equation 3.9
- $Q_{l,w}$  : Wave induced shear force on longitudinal hull girder in head seas, see Equation 3.10

#### DNV

The most unfavourable still water conditions are required by DNV. If the information required for the still water load calculation is not available, the still water longitudinal bending moment for hogging can be assumed with Equation 3.2. Sagging conditions can be assumed zero.

$$M_{y,SW,H} = 0.5\Delta L \quad (3.2)$$

The resulting shear force distribution is not treated individually and is calculated from the longitudinal bending moment with the following equation:

$$Q_{l,SW} = \frac{M_{y,SW,H}}{0.25L} \quad (3.3)$$

The transverse bending moment,  $M_x$ , is also required and is assumed to be:

$$M_{x,SW} = 4.91\Delta (0.5s - 0.4B^{0.88}) \quad (3.4)$$

### 3.1.3 Comparison

The method to determine the still water loads based on first principles requires the hull shape or a buoyancy distribution as well as a mass distribution. The class societies propose simplified methods to get an early estimation of the still water design loads early in the design process when no hull shape is known. These methods are schematically drawn in Figure 3.5.

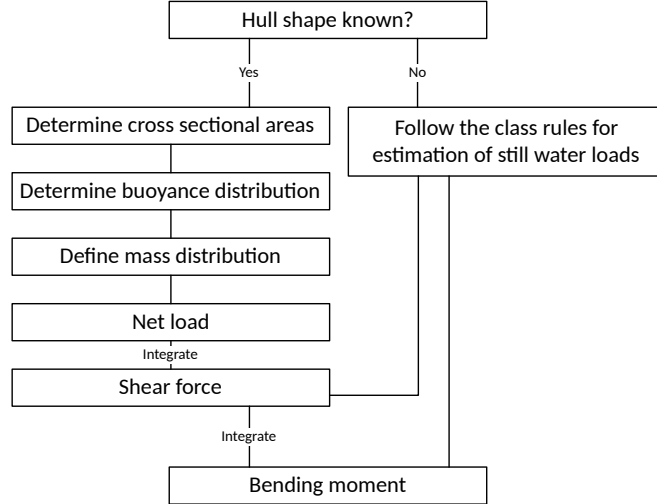


Figure 3.5: Method for defining the still water bending moment

The different methods both determine still water bending moments (SWBM) and shear force distributions. These results are plotted in Figure 3.6. From the results, it can be seen that the estimation of the bending moment by Bureau Veritas is conservative but relatively useful as the maximum bending moment is 25% larger than the result based on first principles. The estimation made by the DNV rules is not useful as the maximum bending moment is 147% larger than the maximum SWBM for the concerning hull shape. The still water shear force results are shown in Figure 3.6a. The BV positive estimate is 19% larger than the maximum calculated value while the negative estimate is 2% smaller than the absolute minimum value, however, the distribution is off. The distribution used by BV assumes a maximum and minimum shear from  $0.3L$  to  $0.7L$  aft, while the minimum shear value occurs outside this region at  $0.75L$ . The DNV estimate is 197% larger than the maximum value and 146% larger than the minimum value. This makes the DNV estimation not realistic for this vessel.

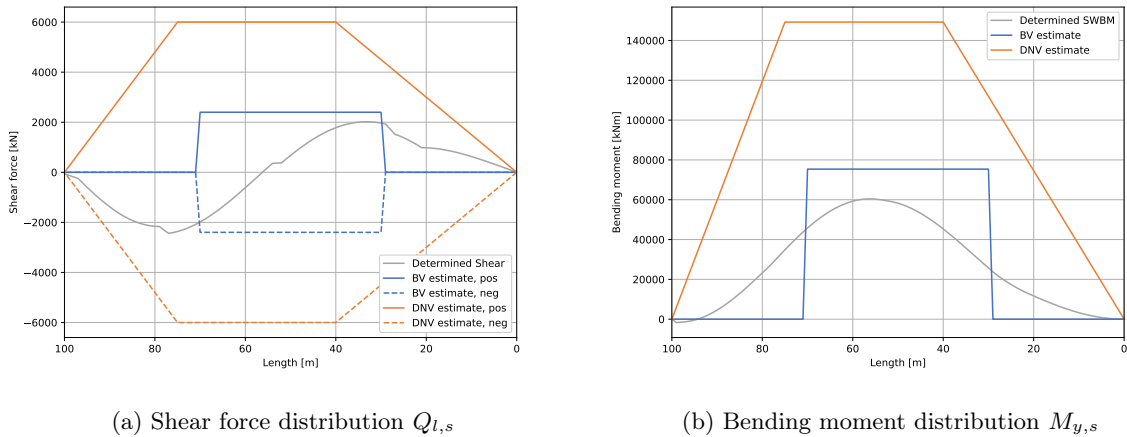


Figure 3.6: Still water load case results comparison

## 3.2 Wave-induced loads - head seas

When a vessel is sailing at sea it will encounter waves. These waves result in fluctuating pressures on the hull. This changes the buoyancy force resulting in varying moments and loads. These loads are dependent on the shape and direction of the waves. In this section, the vessel in head seas is covered. For designing a vessel, a maximum wave load is determined. This wave load is the most critical wave load the vessel is expected to encounter during its lifetime, based on statistics. The sea's surface appears to be composed of random waves of various lengths. These waves can be described statistically for short periods (around 3 hours), which results in wave spectra. The long-term description of the sea surface is a combination of many wave spectra combined in one scatter diagram.

This critical wave load can be found with full-scale experiments, with model testing and scaling factors or with numerical methods. However, full-scale experiments are impossible as no ship resembles the design vessel of this research. Model tests could be useful but are expensive and time-consuming, which is not desirable in the concept design phase.

In this section, the wave-induced loads resulting from head seas are determined. The first principles are analyzed and then a method for determining the load based on the first principles is proposed. This method uses a static wave which requires a certain wave height which is examined next. In the second subsection, the load is determined according to the guidelines of the classification societies. The result of the static wave method is then compared with the results from the class societies.

### 3.2.1 First principles

The largest wave loads are a result of the most critical waves. Each moment or shear force reaches its highest value for different ship motions as a result of different waves. To obtain these values the vessel's hydrodynamics are of importance. To describe all fluid-structure interactions between the waves and the vessel the governing equations of the motion of the vessel, the governing equations of the waves alone and the interaction condition need to be solved. For short periods of time, for example, one wave or a measured sea state, Computation Fluid Dynamics (CFD) can be used for defining the wave-induced loads using Reynolds Averaged Navier Stokes (RANS) equations. This is computationally expensive and requires more actual time than the modelled time span[13]. This makes it impossible to use these full velocity potential equations to find the maximum load of the vessel during the whole lifespan of the vessel. Instead, an approximation of the interactions is made that only looks in the longitudinal direction. This strip theory was first designed for monohulls but was later adapted for catamarans [9][18][11]. A potential flow theory is developed for catamarans to also include the transverse direction[14][5][21]. When the vessel's hydrodynamics are known from a strip theory or potential flow theory, they can be converted to Response Amplitude Operators (RAO), which give a linear relationship between the wave spectrum and the response of the vessel. The resulting response spectrum shows the movements of the vessel, which can be translated to pressure distributions over the hull. The most severe pressure distribution results in the load case. The above methods are time and computational expensive and are based on the exact hull design and mass distributions. This makes these methods not ideal for early on in the design process.

In this research, the wave-induced load will be determined by applying a static wave to the hull. This wave will result in a pressure distribution over the hull resulting in a load case. This wave's height and length are crucial and determined in the next section. The load case for the vessel in head seas is determined as well.

### 3.2.2 Static wave load

In order to find the maximum moments and resulting stresses, the critical wave conditions need to be determined. The sea surface can be assumed stationary for short-term descriptions of the sea, ranging from 20 minutes to 3-6 hours. A wave spectrum can describe the stationary surface with two environmental parameters: the significant wave height and the peak period. However, the sea cannot be described as a stationary process for long-term descriptions of the sea. For the long-term description, scatter diagrams are available of multiple areas, which show a joint probability distribution of the wave height and the peak period. The fatigue limit state can be based directly on these scatter diagrams[7]. The critical wave conditions are different for each moment and shear force. The longitudinal bending

moment,  $M_y$ , and vertical shear on the longitudinal hull girder,  $Q_l$ , are most critical in head seas with a wavelength around the ship's length. The maximum wave height is limited for each wavelength. Miche (1944) has theoretically shown that the wave steepness of a harmonic wave is finite. The maximum wave height is determined by the speed of the crest, which cannot be larger than the speed of the wave without breaking. This results in the following upper limit:

$$H_{\max} \approx 0.142L \tanh\left(\frac{2\pi d}{L}\right) \quad (3.5)$$

Where:

$H_{max}$  : max. wave height  
 $L$  : wavelength  
 $d$  : depth

In deep water, the maximum wave height is thus equal to  $0.14L$ . However, this is the physical maximum wave height and is a wave height that will never be met, especially for larger wavelengths. Therefore, the largest wave height that will be used for the analysis is statistically determined. The irregular surface of the sea can be divided into many regular waves with different amplitudes, frequencies and directions that together form the irregular surface. This rough surface can be converted into a wave spectrum. Different sea states result in different wave spectra. For this design, a sea state of 7 is selected. This is a severe sea state with a probability of occurrence of 6.1% in the Northern Atlantic[16]. The higher sea states 8 and 9 have a probability of  $< 1.25\%$ . However, the ship will avoid these most severe sea states. For each of these sea states, the most probable significant wave height  $H_{1/3}$  and peak period  $T_p$  are given, see Table 3.1. Also, the most critical combination, which has a much lower probability, is presented[16][1].

The wave heights are given for two wavelengths: head seas and quartering seas. In head seas, the most critical situation is waves of the same length as the vessel, so 100m. In beam seas, the most critical condition is unclear as most loads in beam seas result from roll motion, which is not taken into account by a static wave. For catamarans, quartering sea conditions are critical as they result in the pitch connecting moment,  $M_p$ . The most critical wavelength in quartering seas occurs when the wave troughs go through the diagonal tips while the wave crest goes through the other diagonal tips, see Figure 3.7.

$$L_{WQ} = \frac{2L_{wl}s}{\sqrt{L_{wl}^2 + s^2}} = 45.29m \quad (3.6)$$

Sea state	$H_{1/3}$	$T_p$	H for L=100m	H for L=45.3m
6 most critical	6m	9.8s	5.44m	2.49m
7 average	7.5m	15s	3.67m	1.39m
7 most critical	9m	11.8s	6.54m	2.65m
8 average	11.5m	16.4s	4.79m	1.79m
8 most critical	14m	14.2s	7.55m	2.89m
9 average	14m	20s	4.00m	1.47m
9 most critical	16m	15.7s	7.22m	2.71m

Table 3.1: Wave heights for waves with lengths of 100m and 45.3m. Sea states according to NATO STANAG 4194.[16]

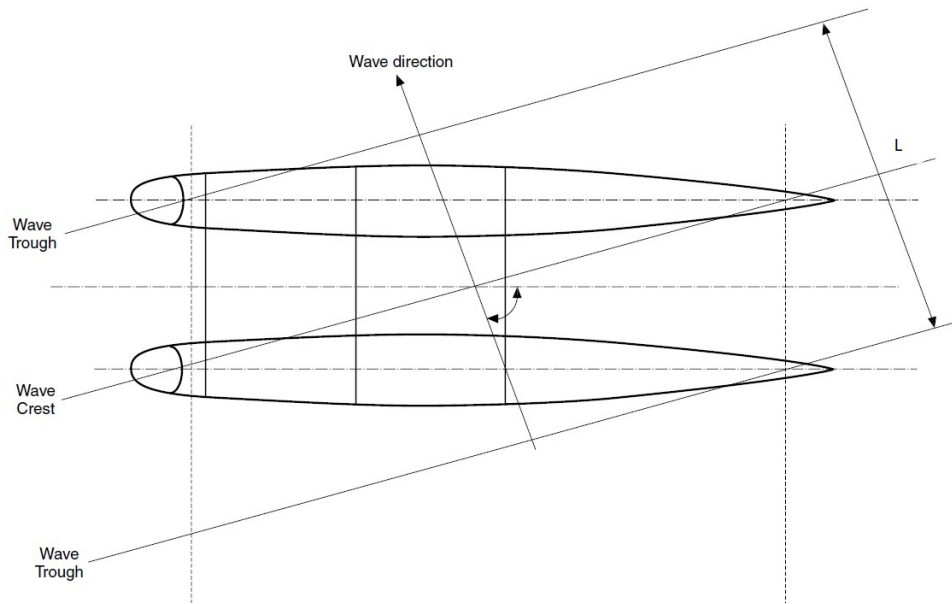


Figure 3.7: The most critical wavelength for quartering sea waves [4]

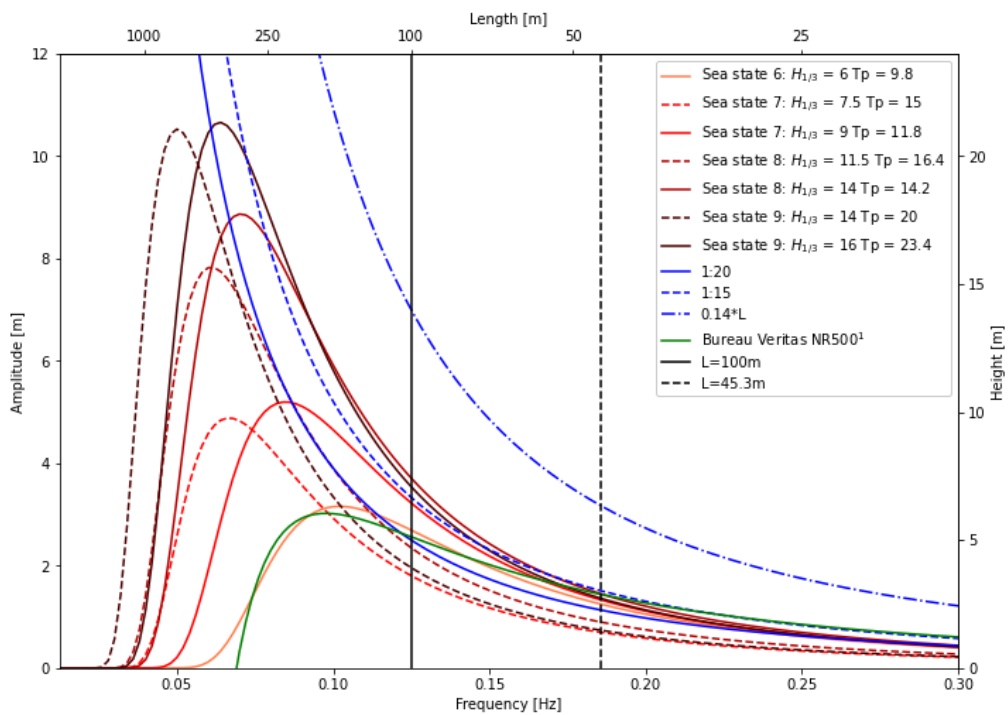


Figure 3.8: Bretschneider wave spectra of different sea states <sup>1</sup>Bureau Veritas NR500 rules are limited to a length of 100m

A Bretschneider wave spectrum, also called the modified two-parameter Pierson-Moskowitz wave spectrum, can be computed with the specific wave heights and peak periods. The energy density spectra are converted to spectra of amplitude over wave frequency. The deep-water dispersion relations can relate a particular wave frequency to a wavelength. The wave spectra are plotted together with the physical maximum wave amplitude and the wave amplitude according to Bureau Veritas NR500[4], see Figure 3.8.

The different wave spectra in Figure 3.8 show that the average significant wave height and peak period of a certain sea state result in lower wave heights than the most critical combination of a lower sea state. The most critical values of the sea states converge to one point, and the spectra of the average values of different sea states combine to one point as well for smaller wavelengths. The wave height of Bureau Veritas is higher than the sea state spectra at smaller lengths. However, at lengths of 50m and larger, the given design wave height is almost equal to the most critical sea state 6, as can be seen in Figure 3.8. This is most likely because Bureau Veritas estimates that yachts will not encounter these severe sea states of 7 or larger, as yachts will always avoid these extreme storm conditions. Sea state 8 is typical for most hurricanes and is used as the general criterion for U.S. navy ships[20]. The common rule of practice with a wave steepness of 1:20 is lower than the design wave height given by Bureau Veritas at lower lengths and also seems low compared to the shown sea states. However, at a wavelength of 100m, it almost equals the wave height provided by Bureau Veritas. A wave steepness of 1:15 seems to follow the wave height given by Bureau Veritas much better at lower wavelengths and is more conservative at larger wavelengths. The wave height probability histogram of area 43, the Northern Pacific, Figure 3.9 shows that the conservative wave steepness of 1:15 includes the most unlikely waves. In contrast, the wave steepness of 1:20 does not include these waves, especially at the critical wavelengths. For this research, the conservative wave steepness of 1:15 will be used. This results in the design wave parameters as given in Table 3.2.

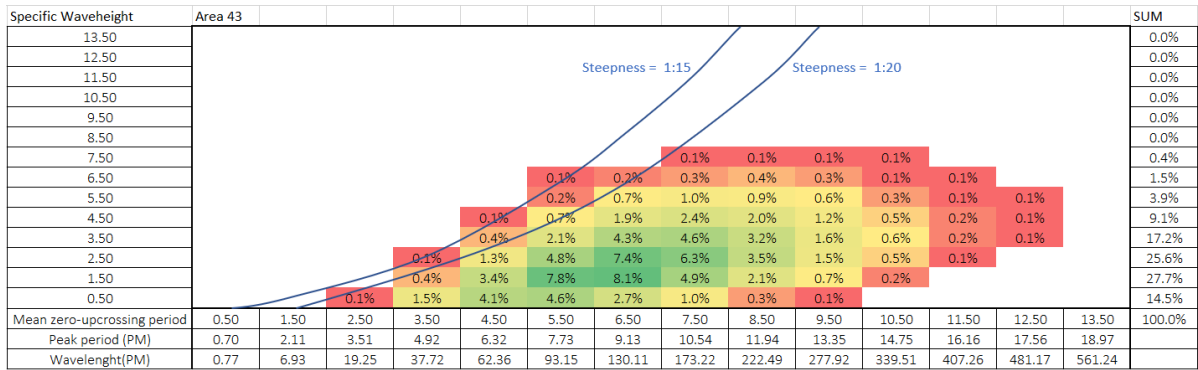


Figure 3.9: Wave height probability histogram of area 43, Northern Pacific

Table 3.2: Design wave parameters

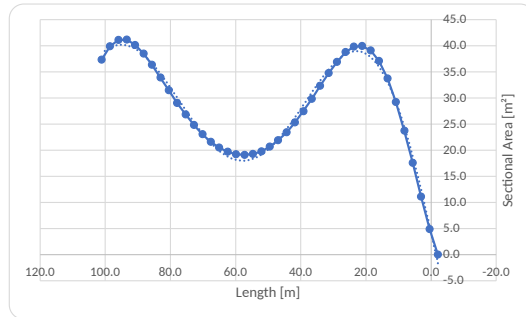
Wave direction	Wavelength	Wave height
Head seas	100m	6.66m
Quartering/oblique seas	45.44m	3.03m

### Static wave results

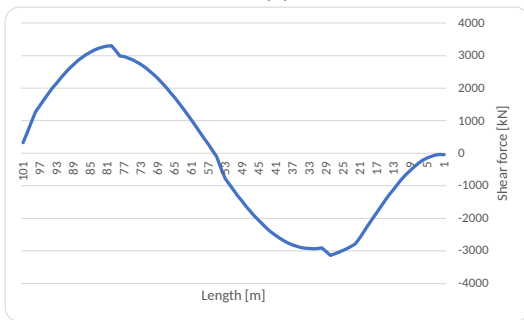
As shown above, the most critical conditions in head seas occur when the wavelengths are around the vessels' waterline length. In head seas, the static waves, with the parameters shown in Table 3.3, are subjected to the hull. The method to define the shear force and bending moment distributions resulting from this wave is equal to the procedure for defining the still water wave load, see subsection 3.1.1. This method integrates the net load once to obtain the shear force distribution and once more to get the bending moment distribution. The crest of the wave is shifted by a few meters, see the phase column in Table 3.3, to keep the trim of the vessel at zero degrees. The head sea shear force for sagging is shown in Figure 3.10b and the head sea longitudinal bending moment for sagging in Figure 3.10c, the hogging conditions are shown in Figure 3.11. When the vessel is on top of a wave crest in head sea conditions, a positive vertical bending moment,  $M_y$ , results in a so-called 'hogging' condition. When the vessel is in a wave trough, the vertical bending moment is negative and results in a 'sagging' condition.

Table 3.3: Head sea static wave parameters

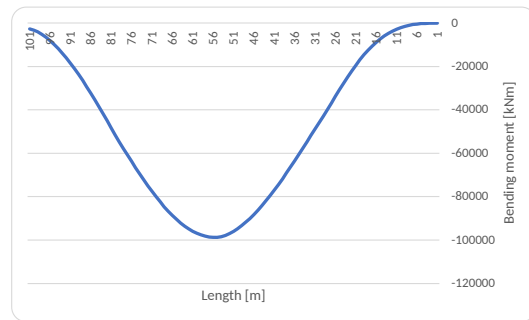
Resulting motion:	Wavelength:	Wave height:	Phase:	Angle of attack:
Sagging	99.49	6.63	22°	0°
Hogging	99.49	6.63	190°	0°



(a) Buoyancy as a result of the applied static sagging wave

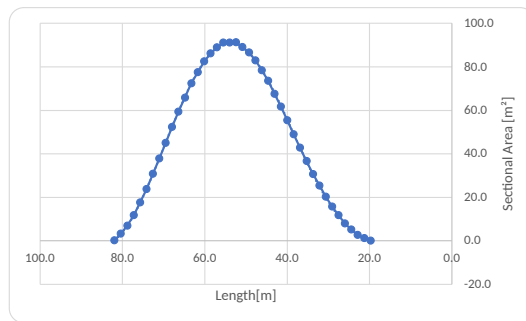


(b) Head sea sagging shear,  $Q_{l,w}$

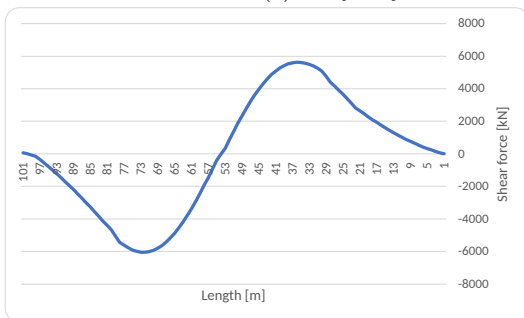


(c) Head sea sagging bending moment,  $M_{y,w}$

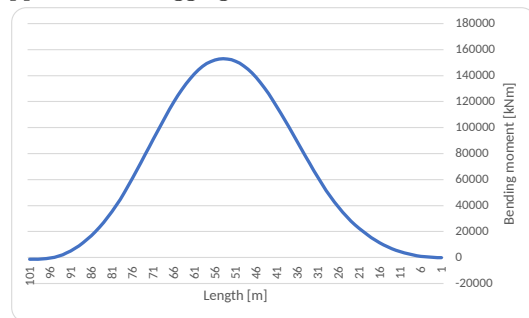
Figure 3.10: Head sea sagging conditions



(a) Buoyancy as a result of the applied static hogging wave



(b) Head sea hogging shear,  $Q_{l,w}$



(c) Head sea hogging bending moment,  $M_{y,w}$

Figure 3.11: Head sea hogging conditions

### 3.2.3 Class based guidelines

The class societies use a deterministic approach to determine the loads. They provide approximate formulas for the wave longitudinal bending moment,  $M_{y,w}$  and shear force distribution,  $Q_{l,w}$ . The IACS (International Association of Classification Societies) has not yet standardized these formulas for large catamarans. This results in various formulas for this vessel type from the different class societies. Before the classification societies had rules for large catamarans, the U.S. Ship Structure Committee assembled a report (1971) with very conservative rules for the critical loads of large catamarans and other twin-hulled ships[19].

#### ABS

ABS provides equations for the wave bending moments in both sagging and hogging conditions[2].

$$\begin{aligned} M_{y,ws} &= -110C_1L_{wl}^22B_{wl}(C_b + 0.7) \times 10^{-3}(\text{kNm}) \text{ Sagging Moment} \\ M_{y,wh} &= 190C_1L_{wl}^22B_{wl}C_b \times 10^{-3}(\text{kNm}) \text{ Hogging Moment} \end{aligned} \quad (3.7)$$

Where:

$$C_1 = 0.044 \cdot L + 3.75$$

Wave-induced longitudinal positive and negative shear force distribution:

$$\begin{aligned} Q_{y,wp} &= +30F_1C_1L_{wl}2B_{wl}(C_b + 0.7) \times 10^{-2}(\text{kN}) \\ Q_{y,wn} &= -30F_2C_1L_{wl}2B_{wl}(C_b + 0.7) \times 10^{-2}(\text{kN}) \end{aligned} \quad (3.8)$$

Where:

$F_1$  &  $F_2$  : distribution factors

The method is followed and Equation 3.7 is filled in. This results in the bending moments shown in Figure 3.12b. The sagging bending moment is significantly larger than the hogging bending moment due to the +0.7 element in Equation 3.7. When the still water bending moment is added, the sagging moment will reduce while the hogging moment increases. The shear force is determined according to Equation 3.8 and shown in Figure 3.12a.

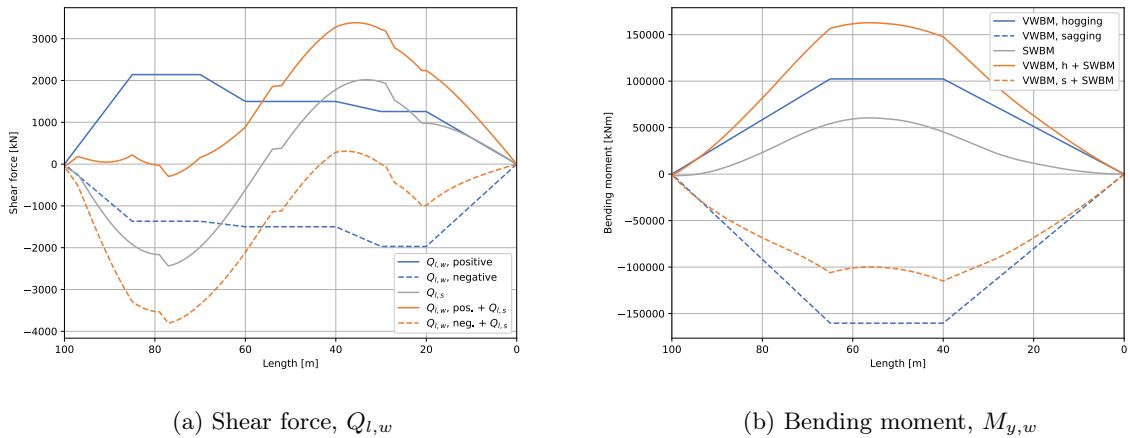


Figure 3.12: wave-induced loads in head seas, according to the American Bureau of Shipping

## Bureau Veritas

According to NR500 by BV, the global wave loads are defined in head sea conditions with the following equations. There is a correction factor for sailing catamarans of plus 30% and the loads are doubled to get a total load of both semi-hulls.

$$M_{y,w} = 0.20nH_WL_{WL}^2B_{WL}C_B \cdot 1.3 \cdot 2(\text{kNm}) \quad (3.9)$$

$$Q_{l,w} = 0.65 n H_W L_{WL} B_{WL} C_B \cdot 1.3 \cdot 2(\text{kN}) \quad (3.10)$$

Where:

- $n$  : Navigation coefficient (=1 for unrestricted vessels)
- $H_W$  : Wave height, in m
- $L_{WL}$  : Wavelength, in m
- $B_{WL}$  : Maximum breath at waterline of one float, in m
- $C_B$  : Total block coefficient

$$H_W = 0.625 (118 - 0.36 L_W) L_W 10^{-3} \quad (3.11)$$

The load is applied from  $0.3L_{WL}$  to  $0.7L_{WL}$ , which results in a 'square' distribution, see Figure 3.13. The hull girder loads outside this region are overlooked and considered equal to zero. The overall bending moment induced by still water and wave loads is in hogging the summation of  $M_{y,w}$  and  $M_{y,s}$ , while in sagging it is only the negative value of  $M_{y,w}$ . The results are given in Figure 3.13.

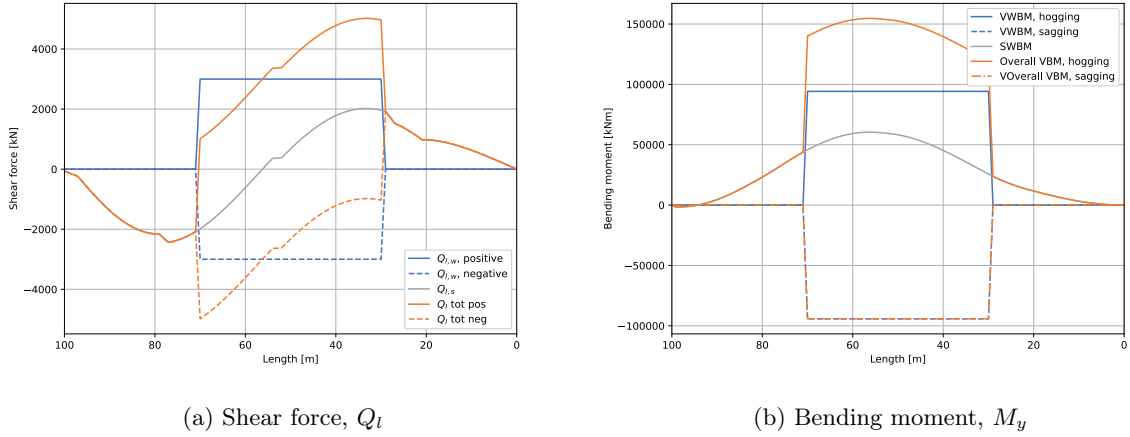


Figure 3.13: wave-induced loads in head seas according to Bureau Veritas

## DNV

The maximum longitudinal bending moment for twin-hull vessels is given by DNV for hogging and sagging conditions. This maximum value is distributed over the length with a distribution factor between one and zero.

$$M_{y,w,max} = 0.19C_wL_{wl}^2(2B_{wl} + k_2B_{tn})C_B(\text{kNm}) \text{ in hogging} \quad (3.12)$$

$$0.14C_wL_{wl}^2(2B_{wl} + k_3B_{tn})(C_B + 0.7)(\text{kNm}) \text{ in sagging}$$

$$k_2 = 1 - \frac{z - 0.5T}{0.5T + 2C_W}, \text{ minimum } 0 \quad (3.13)$$

$$k_3 = 1 - \frac{z - 0.5T}{0.5T + 2.5C_W}, \text{ minimum } 0$$

Where:

- $C_w$  : wave coefficient
- $z$  : height in m from canoe line to wet deck

For unrestricted service:

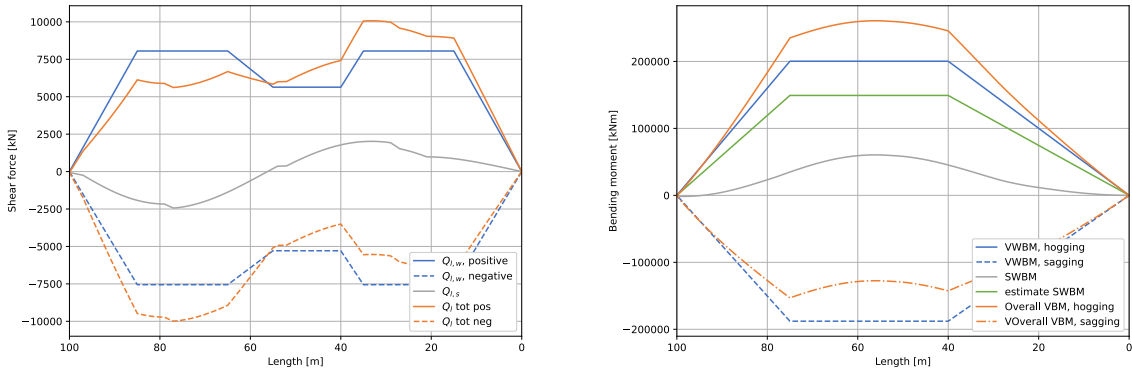
$$C_W = 0.08L_{wl} \text{ for } L_{wl} \leq 100 \text{ m} \quad (3.14)$$

$$= 6 + 0.02L_{wl} \text{ for } L_{wl} > 100 \text{ m}$$

The shear force distribution over the longitudinal hull girder is approximated by the following equation and distributed with a distribution factor.

$$Q_{l,w,max} = \frac{M_{y,w,max}}{0.25L_{wl}} \quad (3.15)$$

The wave bending moment and shear force distribution are shown for the concerning vessel Figure 3.14.



(a) Shear force,  $Q_{l,w}$

(b) Bending moment,  $M_{y,w}$

Figure 3.14: Wave-induced loads in head seas according to Det Norske Veritas

## ISO

The rules by ISO are for small craft multihulls (ISO 12215-7:2020). For small craft, the global loads are of less importance. This is why these rules do not provide equations for longitudinal bending and shear.

## Lloyd's Register

The 'Special service craft' rules provide specific regulations for catamarans and other multihulls like SWATHs. Both equations for the wave bending moment and wave shear force include the still water effects, which is why the still water loads are not summed.

Wave bending moment distribution for sagging and hogging:

$$M_{y,w} = F_f D_f M_M (\text{kNm}) \quad (3.16)$$

$$F_f = -1.0 \text{ for sagging moment} \quad (3.17)$$

$$= 1.0 \text{ for hogging moment}$$

$$M_M = S_f \times G_f \times E_f \times C_{WP} \times L_R^2 \cdot 5 \times 2B_{wl} (\text{kNm}) \quad (3.18)$$

$$E_f = 0.125 \text{ for sagging moment} \quad (3.19)$$

$$= 0.2 \text{ for hogging moment}$$

Where:

- $D_f$  : distribution factor over the length
- $S_f$  : cargo factor (passenger = 1.1)
- $G_f$  : service group factor
- $C_{WP}$  : waterplane area coefficient (taken not less than 0.5)
- $L_R$  : Rule length

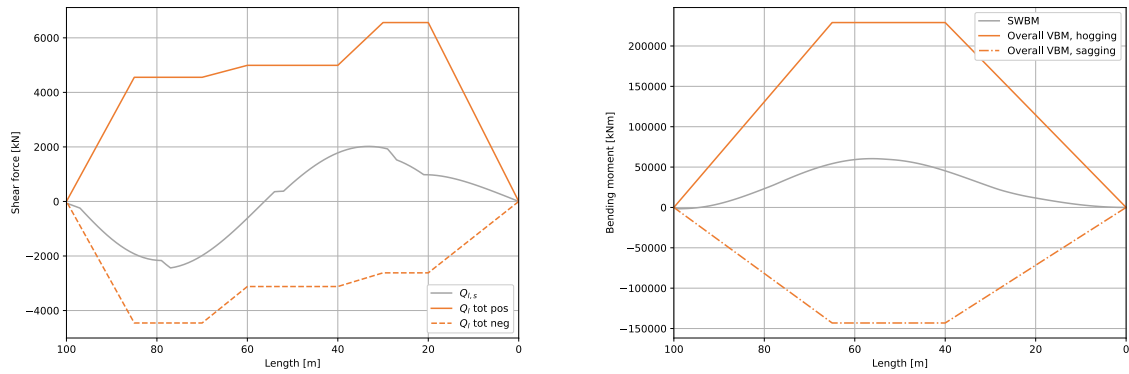
Wave shear force distribution, both positive and negative:

$$Q_{l,w} = \frac{3K_f M_M}{L_R} (\text{kN}) \quad (3.20)$$

Where:

- $K_f$  : shear force distribution factor over the length

For the concerning vessel, the wave bending moment is shown in Figure 3.15.



(a) Shear force,  $Q_{l,w}$

(b) Bending moment,  $M_{y,w}$

Figure 3.15: Wave-induced loads in head seas, according to Lloyd's Register

### 3.2.4 Comparison

As seen in the previous section, all class societies make use of different parameters to form the same load cases. However, the parameters can be grouped into different categories and then it can be seen that almost all societies use at least one parameter per category, see Table 3.4. The category type of cargo is however only used by Lloyd’s Register. Looking at the physical meaning of the loads, this category is not necessary to include, and is probably added for other reasons, like economic risks. ABS, BV and DNV implement the length for determining the shear force distribution and use the length square to determine the longitudinal bending moment. They also include a wave height/coefficient that is also partially based on the length. Lloyd’s Register does not do so but implements the length to the power 1.5 and 2.5 for the shear force and bending moment, respectively. DNV has a special rule for calculating  $M_{y,w}$  for twin hulls. Bureau Veritas uses the waterline beam of only one hull. The other Classification Societies use the waterline beam of both hulls and DNV even includes the cross structure with a factor for the effect of cross structure immersion in hogging and sagging waves. Bureau Veritas applies a penalty for sailing catamarans resulting in a 30% increase in the bending moment and the longitudinal shear force. The variations of the maximum shear force and longitudinal bending moment are mainly a result of the different constants used by class societies because the used parameters do not vary much.

Table 3.4: Comparison of parameters used by different class societies for calculating the global loads in head seas,  $M$  tells the parameter is used for the bending moment,  $Q^2$  tells the parameter is used quadratically for the shear force distribution

Parameter:	ABS	BV	DNV	LR
Length	$Q M^2$	$Q M^2$	$Q M^2$	$Q^{1.5} M^{2.5}$
Beam waterline (both floats)	$Q M$	$Q M$	$Q M$	$Q M$
Additional beam			$Q M$	
Block coefficient	$Q M$	$Q M$	$Q M$	
Area/navigation factor		$Q M$		$Q M$
Wave height/coefficient	$Q M$	$Q M$	$Q M$	
Cargo				$Q M$

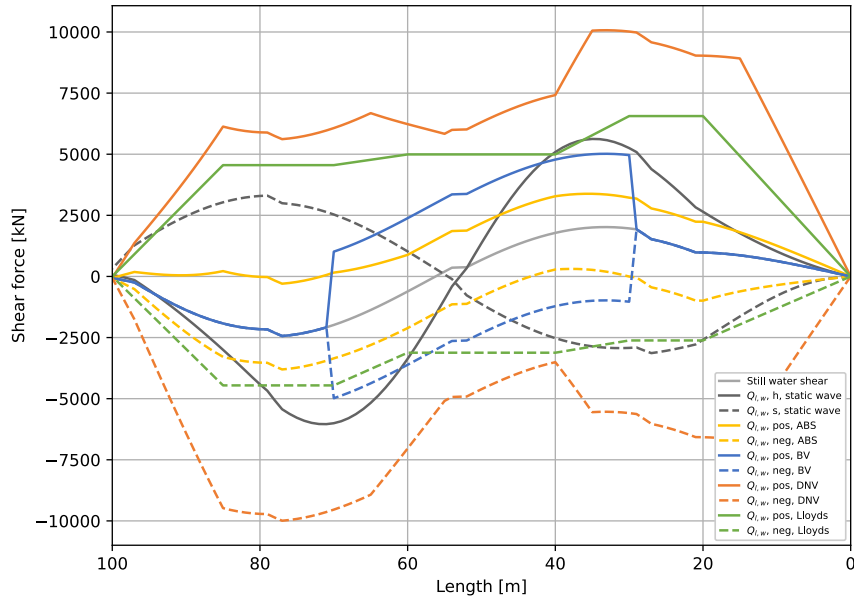


Figure 3.16: Wave-induced vertical shear force in head seas determined according to multiple class societies as well as the static wave approach

The results for the shear force distribution in head seas are shown in Figure 3.16. The most significant difference in maximum shear is between the result from ABS, which is underestimating, and the result from DNV, which is very conservative. The difference is around a factor 3. The envelope of the static wave shows that the shear force is zero in the centre. This only holds for both maximum conditions that are considered. When the wave peak shifts over the length of the hull the maximum shear value also shifts over the length of the hull. The envelope of the static wave method can be extended by drawing a line from both tops. Bureau Veritas also uses a relatively simple distribution envelope. The other Classification Societies have a more varying envelope. The rules of BV from 2016 still do have a relatively similar envelope compared to the other Classification Societies. However, this is simplified in the 'new' rules from 2020.

The results for the longitudinal bending moments in head seas are shown in Figure 3.17. The results from ABS and BV are similar and follow the maximum bending moment determined by the static wave method. The maximum results from DNV and LR are around a factor 2/3 larger than the result from the static wave method. The envelopes of the classification societies increase the length over which the maximum bending moment is applied. The static wave method has only considered two extreme cases. Shifting these cases would results in a broader envelope, but would not increase maximum values.

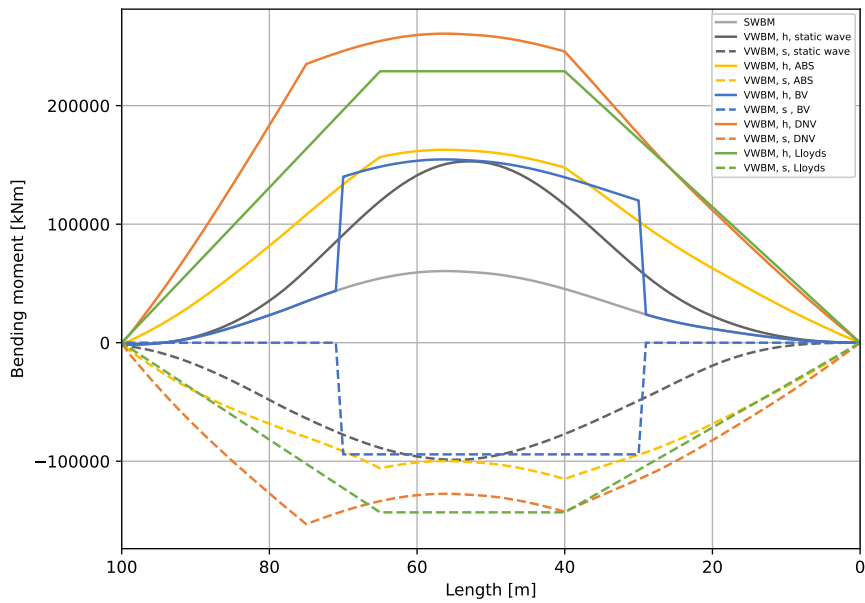


Figure 3.17: Wave-induced longitudinal bending moments in head seas according to multiple class societies as well as the static wave approach

### 3.3 Wave-induced loads - Quartering seas

In this section, the wave-induced loads resulting from quartering waves are determined. The quartering waves will not only act in the longitudinal direction but also in the transverse direction. First, the determination of the load according to the static wave method is shown. Then the results of the class societies are given and compared with the results from the static wave method.

#### 3.3.1 First principles

The static wave method is used to determine the loads based on the first principles. In subsection 3.2.2 this method is explained and the critical wavelength and wave height are determined. The sectional areas required for the buoyancy distribution should be given separately for each demi-hull. This is not possible in the available software. First, the full vessel is placed in the considered wave to find the phase at which the trim and heel are minimal. These waves, shown in Table 3.5, are now applied to both demi-hulls with the required phase shifts. The centre of buoyancy for a single hull in the same wave,

Table 3.5: Quartering sea static wave parameters

Situation:	Wavelength:	Wave height:	Phase:	Angle of attack:	Trim:	Heel:
1	45.3	3.03	95°	76.85°(stbd beam)	0.22°fwd	0.77°stbd
2	45.3	3.03	-79°	76.85°(stbd beam)	0.23°fwd	0.02°port

with equal trim and heel, can now be computed. This needs to be done for both sides. Combining both centres of buoyancy with the centre of gravity results in a torsional moment, see Figure 3.18. The forces are shown in Table 3.6 and it can be seen that both situations result in almost equal forces. This is expected and a result of the symmetry. The errors are a result of rounding errors in the software, which also resulted in the slight heel and trim of the vessel. When the longitudinal centre of gravity (LCG) is taken as the rotation axis, the arm is 7.9m, resulting in a pitch connecting moment,  $M_p$  of  $7.9 \cdot 1462 \cdot 9.81 = 109001\text{kNm}$ .

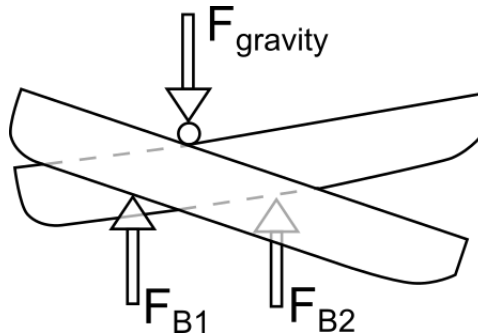


Figure 3.18: Buoyancy forces in quartering sea wave together with gravitational force result in a torsional pitch connecting moment,  $M_p$

Table 3.6: Quartering sea static wave resultant forces

Situation	Hull	Buoyancy force	Location $F_B$	Gravitational force	Location $F_g$
1	PS	1462 m <sup>3</sup>	45	1462 t	53 m
1	SB	1462 m <sup>3</sup>	60.8	1462 t	53 m
2	PS	1462 m <sup>3</sup>	60.7	1462 t	53 m
2	SB	1462 m <sup>3</sup>	44.9	1462 t	53 m

### 3.3.2 Class based guidelines

The different class societies have made guidelines to determine the transverse loads: the transverse bending moment,  $M_x$ , the transverse vertical shear,  $Q_t$ , and the pitch connecting moment,  $M_p$ .

#### ABS

Transverse loading of catamarans:

$$M_{x,w} = 2.5\Delta s (1 + a_{vert}) \quad (\text{kNm}) \quad (3.21)$$

Where:

$a_{vert}$  : max. vertical acceleration, not larger than 7g's

Pitch connecting moment:

$$M_{p,w} = 1.25\Delta L (1 + a_{vert}) \quad (\text{kNm}) \quad (3.22)$$

Transverse shear:

$$Q_{t,w} = 2.5\Delta (1 + a_{vert}) \quad (\text{kN}) \quad (3.23)$$

Vertical acceleration:

$$a_{vert} = 0.0078 \left[ \frac{12h1/3}{B_{WL} * 2} + 1.0 \right] \tau [50 - \beta_{cg}] \frac{V^2 (B_{WL} * 2)^2}{\Delta} g's \quad (3.24)$$

#### Bureau Veritas

The pitch connecting moment in quartering sea resulting in transverse loading is given by:

$$M_p = n H_{wq} L_w^2 B_{wl} C_B \quad (3.25)$$

Where:

- $n$  : Navigation coefficient (=1 for unrestricted vessels)
- $H_{wq}$  : Wave height quartering seas, in m
- $L_w$  : Wavelength, in m
- $B_{wl}$  : Maximum breath at waterline of one float, in m
- $C_B$  : Total block coefficient

$$H_{wq} = 0.625 (118 - 0.36 L_{wq}) L_{wq} 10^{-3} \quad (3.26)$$

$$L_{wq} = \frac{2L_w \cdot s}{\sqrt{L_w^2 + s^2}} \quad (3.27)$$

The wave bending moments and shear forces induced by the wave torque,  $M_{x,t}$ , will be determined by a direct calculation with a 2D beam structure.

#### DNV

The total twin hull transverse bending moment,  $M_x$ , including the still water moment shall be assumed to be the greater of:

$$M_x = M_{x,SW} \left( 1 + \frac{a_{vert}}{g} \right) (\text{kNm}) \quad (3.28)$$

$$M_x = M_{x,SW} + F_y(z - 0.5Tc) (\text{kNm})$$

Where:

- $M_{x,SW}$  : still water transverse bending moment in kNm, see Equation 3.4
- $F_y$  : horizontal split force on immersed hull

$$F_Y = 3.25 \left( 1 + 0.0172 \frac{V}{\sqrt{L}} \right) L^{1.05} T^{1.30} (0.5 B_{WL})^{0.146} \left[ 1 - \frac{L_{BMAX}}{L} + \frac{L_{BMAX}}{L} \left( \frac{B_{MAX}}{B_{WL}} \right)^{2.10} \right] H_1 (kN) \quad (3.29)$$

Where:

- $H_1$  : minimum of 0.143B and  $H_{S,MAX}$
- $H_{S,MAX}$  : maximum significant wave height in which the vessel is allowed to operate, in m
- $B_{max}$  : maximum width of the submerged part
- $L_{Bmax}$  : length in metres where  $B_{max} > B_{wl}$
- $z$  : height from baseline to the neutral axis of the cross structure, in m

Pitch connecting moment

$$M_P = \frac{\Delta a_{vert} L}{8} (kNm) \quad (3.30)$$

Where:

- $a_{vert}$  : max. vertical acceleration, not to be taken less than 9.81 [m/s<sup>2</sup>]

$$a_{vert} = 6 \frac{H s_i}{L} \left( 0.85 + 0.35 \frac{V_i}{\sqrt{L}} \right) 9.81 \text{ ( m/s}^2\text{)} \quad (3.31)$$

## ISO

These rules are for small craft multihulls (ISO 12215-7:2020). For small craft, the global loads are of less importance. This is why these rules do not provide equations for longitudinal bending and shear.

Pitch connecting moment:

$$M_{p,w} = k_{DC}^{0.5} \times \Delta \times (9.81 \times k_{DYNM}) \times 0.076 L_{DIAG} (kNm) \quad (3.32)$$

Where:

- $k_{DC}$  : design category factor, for unrestricted vessels equal to 1
- $L_{DIAG}$  : diagonal length in m
- $k_{DYNM}$  : dynamic load factor

$$L_{DIAG} = \sqrt{L_{WL}^2 + s^2} \text{ ( m)} \quad (3.33)$$

$$k_{DYNM} = \frac{2.5 \times L_{WL}^2}{m_{LDC}^{0.66}} \quad \text{that shall not be taken } < 1 \text{ nor } > 2 \quad (3.34)$$

Where:

- $m_{LDC}$  : mass in kg

Transverse bending moment and shear:

$$M_x = k_{DC}^{0.5} \times \frac{m_{LDC}}{1000} \times 9.81 \times k_{DYNM}^{0.5} \times \frac{s}{8} (kNm) \quad (3.35)$$

$$Q_t = 0.25 \times k_{DC}^{0.5} \times \frac{m_{LDC}}{1000} \times 9.81 \times k_{DYNM} (kN) \quad (3.36)$$

## Lloyd's Register

The guidelines developed by LR all include a service group factor. This factor is based on the service area of the vessel and is different in each equation. In the following guidelines, the service group factor is already filled in for unrestricted vessels.

Transverse bending moment:

$$M_x = 2.5\Delta s a_{vert} (\text{kNm}) \quad (3.37)$$

Pitch connecting moment:

$$M_{p,w} = 1.25\Delta L_R a_{vert} (\text{kNm}) \quad (3.38)$$

Transverse shear:

$$Q_t = 2.5\Delta a_{vert} (\text{kN}) \quad (3.39)$$

Vertical acceleration in  $g$ 's, not to be taken less than 1:

$$a_{vert} = 1.5\theta_B L_1 (H_1 + 0.084) (5 - 0.1\theta_D) \Gamma^2 \times 10^{-3} \quad (3.40)$$

Where:

- $\Gamma$  : Taylor quotient
- $\theta_D$  : deadrise angle at ICG [degrees]
- $\theta_B$  : running trim not to be taken less than 3 [degrees]

$$L_1 = \frac{L_{WL} B_c^3}{B_W \Delta} \quad (3.41)$$

$$H_1 = \frac{H_{1/3}}{B_W}, \text{ but is not to be taken as less than } 0.2 \quad (3.42)$$

### 3.3.3 Comparison

When the above classification guidelines are applied to the vessel specification, the results vary for each class society and each load. The results are shown in Figure 3.19. The transverse vertical shear,  $Q_t$ , determined by both ABS and LR is relatively equal. The result from ISO is not shown as it deviates much and skews the graph. In Table 3.7 the parameters are shown that are used for each load. In this table, it can be seen that ABS and LR use the same parameters. The method by ISO uses very different parameters, the length of the vessel contributes more than the displacement, which is not expected for the transverse shear.

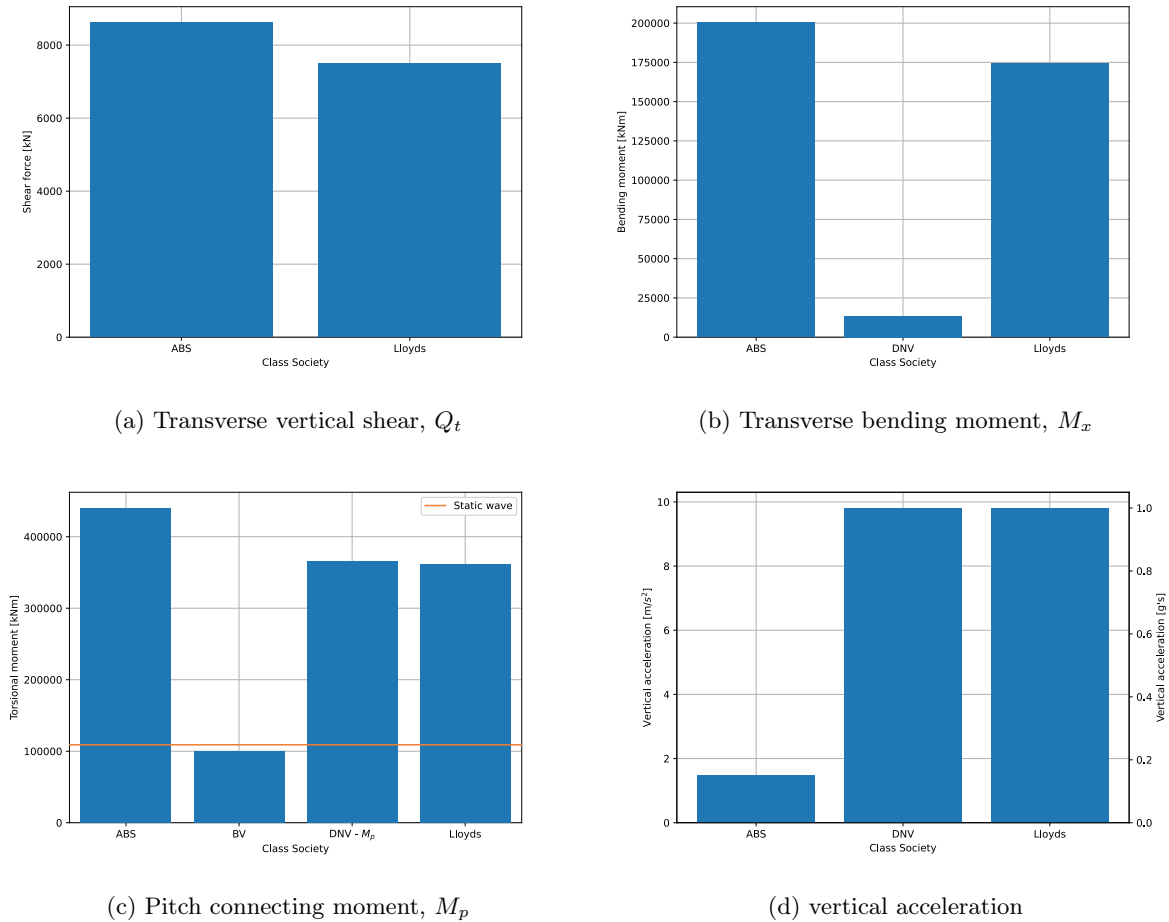


Figure 3.19: The resulting loads for the concerned vessel according to different class societies

The transverse bending moment,  $M_x$ , determined by ABS, LR and DNV varies largely. The moment determined by DNV is ten times smaller than the moment determined by ABS and LR. This significant deviation could result from the different parameters used by the societies. DNV does not take the float centreline separation or the vessel's full beam into account for calculating the transverse bending moment. This dimension however is crucial as a larger separation between the hulls will result in a larger moment. Not all class societies calculate the transverse bending moment and shear force, because they calculate these forces and moments as a result of the more critical pitch connecting moment.

This pitch connecting moment is determined by each class society. The analytical method also provides the pitch connecting moment. Bureau Veritas uses the height of quartering waves in their approach to determine this moment. The analytical method also uses the quartering waves' wave height. The static wave method complies very well with the result from Bureau Veritas. The method from ISO results in a pitch connecting moment almost 300 times larger than the result from the static wave method and the method by Bureau Veritas. Because the method of ISO is limited to vessels of 24m, the subject vessel is far out of this range. Because of the significant deviation, the result from ISO is not taken into account

and removed from Figure 3.19. The other class societies all use a simple equation that multiplies the displacement, the length, the vertical acceleration and a constant, see Equation 3.38, Equation 3.30 and Equation 3.22.

$$M_{p,w} = 1.25\Delta L_{R}a_{vert}(\text{kNm}) \quad (3.38)$$

$$M_P = \frac{a_{vert}}{8}\Delta L(\text{kNm}) \quad (3.30)$$

$$M_{p,w} = 1.25\Delta L(1 + a_{vert}) \quad (\text{kNm}) \quad (3.22)$$

Lloyd's Register uses a vertical acceleration measured in  $g$ 's, with a minimum of 1. ABS also measures the vertical acceleration in  $g$ 's, but the calculated acceleration is much lower which shows in Figure 3.19d. However, in Equation 3.22 the acceleration is summed with one, which is the only difference from the equation from LR. In order to have equal results from LR and ABS the vertical acceleration of LR should be  $1g$  larger than the vertical acceleration of ABS. DNV measures the acceleration in  $\text{m/s}^2$  and divides this by 8, resulting in a value of almost 1.25. The constants used in Equation 3.22 of ABS and Equation 3.38 of LR have an exact value of 1.25. These three class guidelines result in very similar results for the pitch connecting moment, which is around three times larger than the result from the static wave method and Bureau Veritas. This is because ABS, DNV and LR do not make use of the length of the beam in their approaches and do not take the beams of the vessels or the float centre line separation into consideration while this is a key parameter, which can be seen in the static wave approach based on first principles.

Table 3.7: Comparison of parameters used by different class societies for calculating the global loads in quartering seas,  $x$  tells the parameter is used for the transverse bending moment,  $p$  is used for the pitch connecting moment,  $Q^2$  tells the parameter is used quadratically for the transverse shear force

Parameter:	ABS	BV	DNV	ISO	Lloyds
Length	$p$	$p^2$	$x p$	$x^2 p^3 Q^2$	$p$
Float centreline separation	$x$	$p^2$		$x p$	$x$
Max beam waterline (one float)		$p$			
$B_{max}$			$x$		
Displacement	$x p Q$		$p$	$x^{1/3} p^{1/3} Q^{1/3}$	$x p Q$
Draught			$x$		
Block coefficient		$p$			
Vertical acceleration	$x p Q$		$p$		$x p Q$
Max speed			$x$		
Area/navigation factor		$p$			
Wave height/length/coefficient		$p$			

### 3.4 Sail loads

The subject vessel will be equipped with a DynaRig. This free-standing rig results in high local forces and bending moments around the mast bearings. The sail set-up will be a three-masted DynaRig with a total sail area of 3000m<sup>2</sup>. Dykstra Naval Architect has examined the bearing loads as a result of these masts in different circumstances. When the vessel is sailing downwind, it experiences the largest moment around the transverse axis. When the ship is in heavy sea conditions, the largest forces occur in pure roll. However, the bearing forces remain large when the vessel is rolling as well as pitching in wave quartering seas, as can be seen in Table 3.8.

Table 3.8: Bearing loads as a result of different conditions. The difference between the top and lower bearing is 7m.

	$F_x$ [kN] top bearing	$F_x$ [kN] lower bearing	$F_x$ [kN] resultant	$M_y$ [kNm] resultant	$F_y$ [kN] top	$F_y$ [kN] lower	$F_y$ [kN] resultant	$M_x$ [kNm] resultant
Down wind sailing	2426	-1891	535	13,237	0	0	0	0
Roll	0	0	0	0	3618	-2773	845	19,411
Roll & Pitch	1048	-797	251	5579	3185	-2444	741	17,108



Figure 3.20: Superyacht Black Pearl with a DynaRig, by Dykstra Naval Architects and Oceanco. Credit Tom Van Oossanen

### 3.5 Conclusion

The classification societies provide guidelines to approximate the longitudinal bending moment and shear force distribution in still water. The estimate by BV is acceptable. However, the estimate by DNV is too far off. In the concept design phase, it is best to have an estimate of the boundary distribution as a result of the hull shape. This distribution, together with the mass distribution, will determine the actual load in still water conditions.

A static wave method is proposed to determine the load cases resulting from the waves. The method requires a wave height to wavelength ratio that is defined at 1:15. The wave-induced loads in head seas are determined by the class societies and using the proposed static wave method. The results from the classification societies show significant similarities with the static wave method. This makes the static wave method acceptable for determining the loads in head seas during the concept design phase. The sea

state used for the static wave method has very steep waves, resulting in large forces. This compensates for the lack of dynamic forces within the static wave method. The deterministic approaches of the class societies use less severe sea states as they include the dynamic effects.

The transverse structure of the vessel will be critically loaded in quartering waves. The static wave method determined the pitch connecting moment of the vessel, using the critical wavelength and height. BV also uses the wave height and length to determine the pitch connecting moment, and the magnitude of this moment is similar. ABS, DNV and Lloyds use a very simple equation to determine the moment and have a result that is three times larger and very conservative. The static wave method gives a reasonable estimation of the load in quartering seas, and the result will be used for this research. The model used for determining the global wave loads is valuable in the concept design phase.

The sail loads are acting locally on the mast bearings. However, when the transverse structure is analyzed, this additional load should be taken into consideration because the masts are placed in close proximity to these structural elements.

# 4 | Response

In this chapter, the responses as a result of the load cases which are defined in the last chapter are analyzed. The response of the vessel as a result of severe head seas is researched first and focuses on the longitudinal hull structure. The transverse structure is examined in the next section. The critical loading condition for quartering seas are applied to the transverse structure in order to analyze it.

## 4.1 Head seas

The hull shape is simplified by removing all stiffeners and assuming a constant equivalent plate thickness, see Figure 4.1. The hull section is taken at a length of 70.4m aft. Here the longitudinal bending moment is still large and almost equal to the maximum bending as shown earlier in Figure 3.17. However, the height of the hull is less which makes this location more critical than the centre where the height and the stiffness of the hull are both larger. When the hull section has a constant equivalent plate thickness of 8mm, the area moment of inertia around the indicated neutral axis,  $I_y$ , is  $2.1 m^4$ . The furthest fibre distance from the neutral axis,  $z$ , is 3.94m. The longitudinal bending moment is set at 160,000kNm, which follows from the combination of the bending moment calculated according to ABS, BV and the static wave approach, see Figure 3.17. This moment is split over both demi-hulls, resulting in the following equation for one demi-hull:

$$\sigma = \frac{M_B}{2} \cdot z/I_y = 80e6 \cdot 3.94/2.1 = 150MPa$$

Making the hull out of a varying equivalent plate thickness between 15 and 8mm the area moment of inertia,  $I_y$ , becomes  $2.67 m^4$ . The distance to the furthest fibre changes due to the changing neutral axis and becomes 3.89m, see Figure 4.1b.

$$\sigma = \frac{M_B}{2} \cdot z/I_y = 80e6 \cdot 3.89/2.67 = 117MPa$$

With these simplified hull shapes the stress as a result of the longitudinal bending moment in head seas is below the yield stress of aluminium, see Table 1.2. This means that the hull would stay intact in this extreme load case. The normal stress of 150MPa is 30% below the yield stress so the structure can also accommodate for local stresses. As shown above, it is relatively easy to lower the stress even more when required. This can be done by enlarging the plate thickness and implementing additional stiffeners, resulting in a larger equivalent plate thickness. The demi-hull including the three decks has an area of  $3470 m^2$ , resulting in a total area for just both plain hulls without the cross deck of  $6940m^2$ . When executed in a constant equivalent plate thickness of 8mm aluminium the plain hulls have a weight of 148 tons, which is 5% of the total weight.

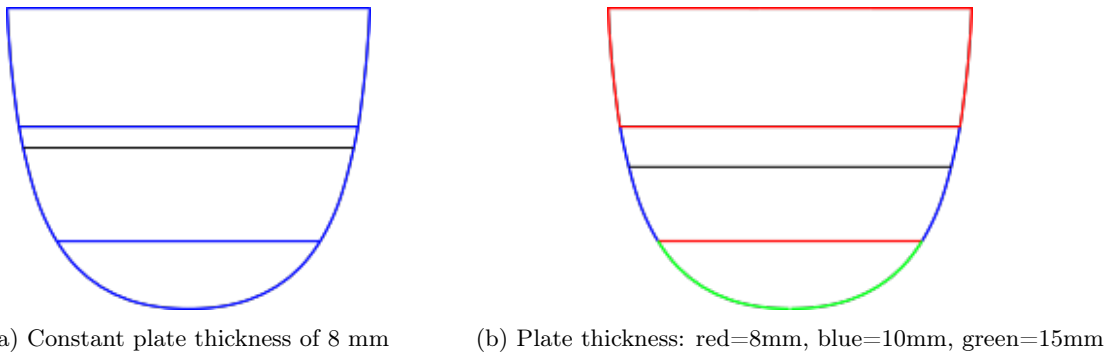


Figure 4.1: Simplified hull cross-section at L=70.4m aft in colour and neutral axis in black

## 4.2 Quartering seas

This section shows the response of the vessel as a result of the implied loads in a quartering sea state. In order to go from the loads defined in chapter 3 to a response, the structure is needed. First, the possibilities for this transverse structure are shown. Then the sail loads are evaluated to see which loads are of importance in this response analysis. Afterwards, a criterion is determined to limit the movement of the structure. The next subsection, subsection 4.2.1, explains the analytical beam model and the energy approach, which results in a response. This method is validated and compared in the follow-up subsection with a computational finite element analysis.

### Transverse structure design

The cross-deck which connects both demi-hulls can be modelled as a multi-cell of torsion boxes between the wet deck and first deck. The first and second deck are connected in four places by a shear web (blue lines) resulting in four possible places for beam elements. Between the middle beam elements, a torsion box can be constructed with the use of both decks. In Figure 4.2 a side view of the vessel is given where the room for such torsion boxes and beam elements is drawn. With thicker lines, the cross deck is drawn to make a clear difference with both demi-hulls which are also drawn.

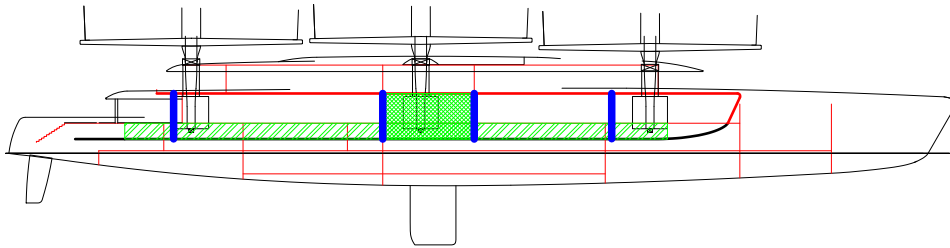


Figure 4.2: Possibilities for global scantlings design. Green shows room for torsion boxes. Blue shows the place for beam elements. Reds are bulkheads and decks.

### Load case

In severe quartering seas, the load case subjected to the structure is combined with the wave-induced load and the sail load. The torsional moment implied on the vessel by the quartering waves as determined in section 3.3 is the driving load case. However, as a result of the rigging, there is a possible additional local load applied to the beams. The fore and mizzen (aft) mast are located near the most fore and aft beam, as can be seen in Figure 4.2. So the additional load from these masts will be applied to these beams, if they are the strongest elements in that direction.

The resultant force forward,  $F_x$ , and the moment around the y-axis,  $M_y$ , see Table 3.8, will be carried by the decks, as the beams are weak in the longitudinal direction. The transverse force,  $F_y$ , will be carried by the beams and will result in a small addition in normal stress. The moment around the x-axis,  $M_x$ , acts in the same plane as the bending moment resulting from the wave torsional moment. This moment is constant over the length of the beam as it is a pure bending moment with no shear force. Both bending moments can be added to find the maximum stress.

Because the sail load is a result of the Roll & Pitch motion, both masts will move in the same direction. The resulting 'sail' bending moments will have the same direction. The wave bending moment as a result of the wave-induced torsion is opposite in direction between both beams. So on one beam, both bending moments add up, while on the other beam they are subtracted from each other.

### Stiffness criterion

Due to the large width of the vessel, the stresses in the torsion boxes can be relatively low (below the yield stress for shear) while the deformations are large, i.e., rotation of more than 10 degrees. So the design of the global transverse structure should not be focused on strength alone as it is also stiffness driven. The large rotational deformation should be prevented in order to keep the other elements of the vessel from braking. For a strength-driven design, the criterion is fairly simple as the stress should

not exceed the yield stress including some safety factor. For this stiffness-driven design, the rotation as a result of the torsional moment will be the criterion. The limiting factor in these vessels is often the large windows in the superstructure as these will break instead of give. The maximum deformation over the diagonal of a window is set at 10mm which is a limit that can still be absorbed by the window caulking.

To determine the value of the maximum rotation, a superstructure, made for an earlier design of the subjected vessel, is modelled relatively flexible by placing it on a much stiffer plate. This stiff plate has been given various fixed rotation angles. So a fixed deformation is applied to the superstructure as the superstructure has no global load carrying capacity. In Figure 4.4 it can be seen that the superstructure is relatively flexible as the stress in the plate is much higher due to the high stiffness. To be able to determine the deformation over the diagonals, flexible beam elements are inserted in all windows. These beams have a Young's modulus of 1Pa and a radius of 5mm. The aluminium in the superstructure has a Young's modulus of 70GPa and a varying plate thickness between 8 and 40mm. The stiff plate has a modulus of  $70e^6$ GPa and a thickness of 10mm. The strain in the beams times their length gives the deformation over the diagonal. In Figure 4.5 the window openings including the flexible beam elements with their strains are shown. The most critical window opening is the window where the deformation is the largest. For this superstructure, the critical 'window' is the glass sliding door located aft, which is the large opening in Figure 4.5. The next critical window opening is located on the side of the vessel and the deformation is around 27% smaller. This shows that the order of magnitude is right for these superstructures and not based on one outlier. The deformation of this most critical window is plotted over the torsional rotation of the stiff plate, see Figure 4.3. A trendline is plotted as well which shows the almost linear relation between the deformation and the rotation at this scale. To limit the deformation at 10mm the maximum torsional rotation is limited at  $0.36^\circ$  over the full beam of the plate of 32m. This gives a maximum twist rate of 0.011 degrees per meter. The maximum rotation over the centreline separation is  $0.26^\circ$  and over the distance between both hulls  $0.16^\circ$ .

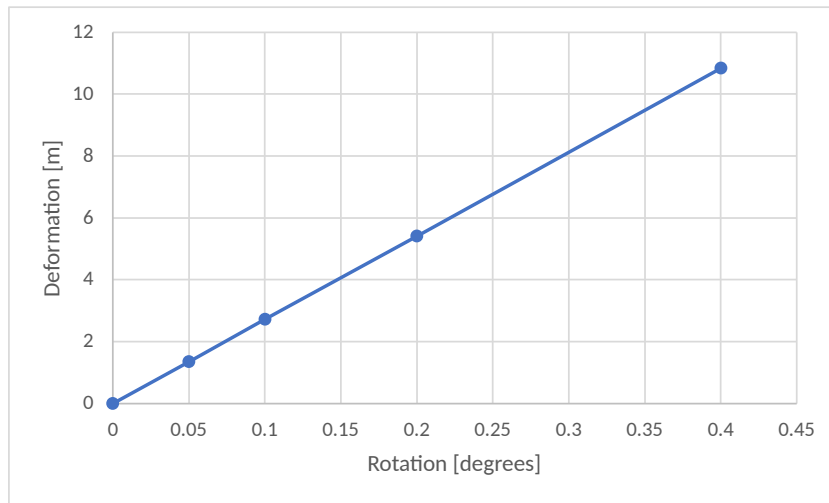


Figure 4.3: Deformation of diagonal of most critical window opening over the torsional rotation of the full superstructure.

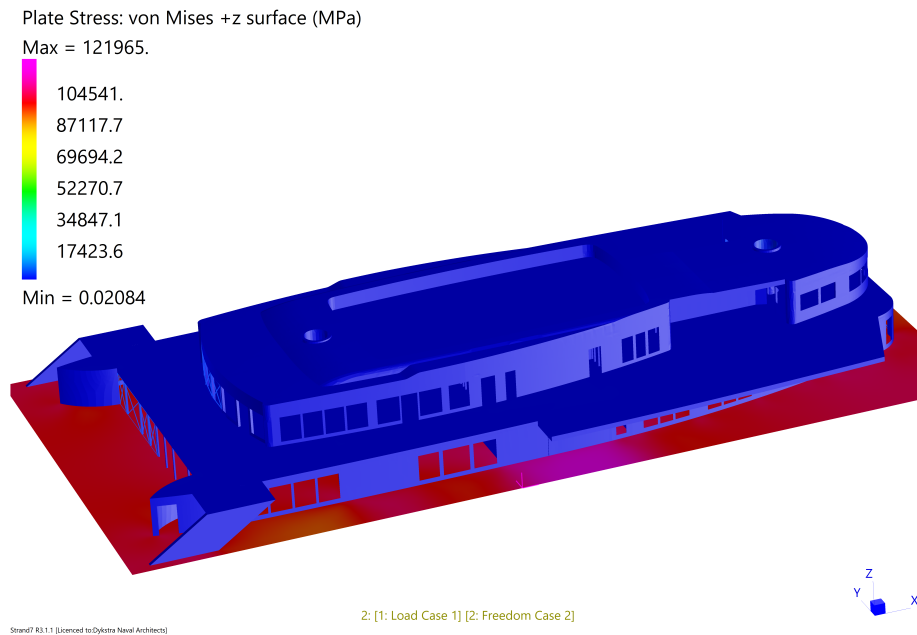


Figure 4.4: Superstructure modelled in FEA on the stiff plate

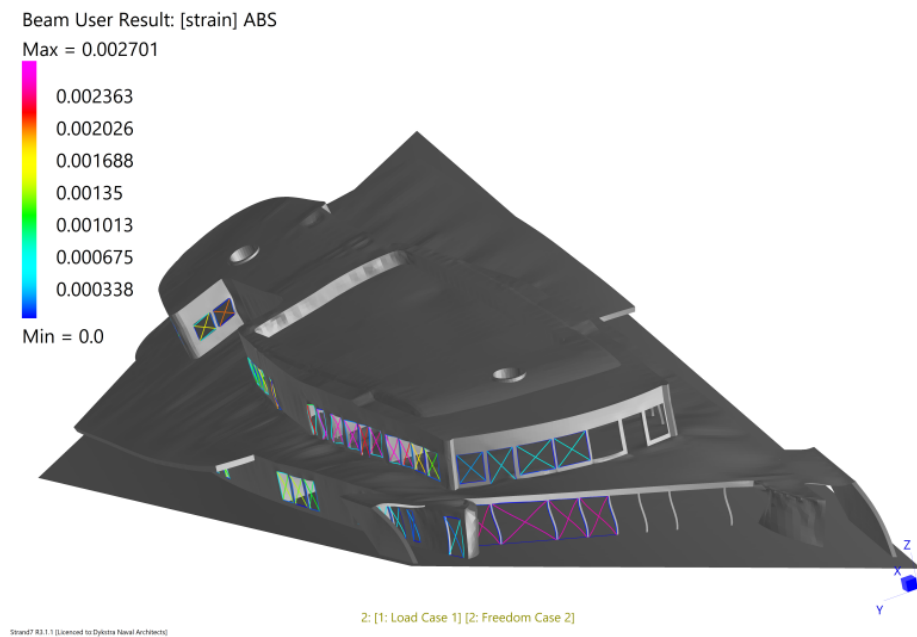


Figure 4.5: Superstructure modelled in FEA shown from the AFT with large openings with high deformations

#### 4.2.1 Analytical model

The transverse structure will be subjected to the previously determined loads. The response will be analytically determined with the use of beam and torsion theory. The used method is based on the conservation of energy. The work done by the applied torsional moment equals the total work done by

the transverse beams and torsion boxes.

$$U_B + U_T = M_p \cdot \theta \quad (4.1)$$

The Euler-Bernoulli beam theory is used to analyze the transverse beams. This theory assumes that the beam is thin and ignores the shear deformations as well as the rotational inertia. The transverse beams are assumed to be fixed at both ends in five degrees of freedom. The beam ends are only allowed to move in the vertical direction. When the torsional moment is applied on the assumed infinite stiff hulls this results in a vertical force on these beams. Direct integration of a beam with the boundary conditions as stated below and a force applied on one end results in the responses shown in the equations below and in Figure 4.6.

Applied boundary conditions:

$$\begin{aligned} \nu(0) &= 0 \\ \theta(0) &= 0 \\ \theta(B) &= 0 \end{aligned}$$

Shear:

$$V(y) = F \quad (4.2)$$

Bending moment:

$$M(y) = \int V(y)dy = Fy - \frac{FB}{2} \quad (4.3)$$

Rotation:

$$\theta(y) = \int \frac{M(y)}{EI} dy = \frac{1}{EI} \left( \frac{1}{2} Fy^2 - \frac{FB}{2} y \right) \quad (4.4)$$

Displacement:

$$\nu(y) = \int \theta(y) dy = \frac{1}{EI} \left( \frac{1}{6} Fy^3 - \frac{FB}{4} y^2 \right) \quad (4.5)$$

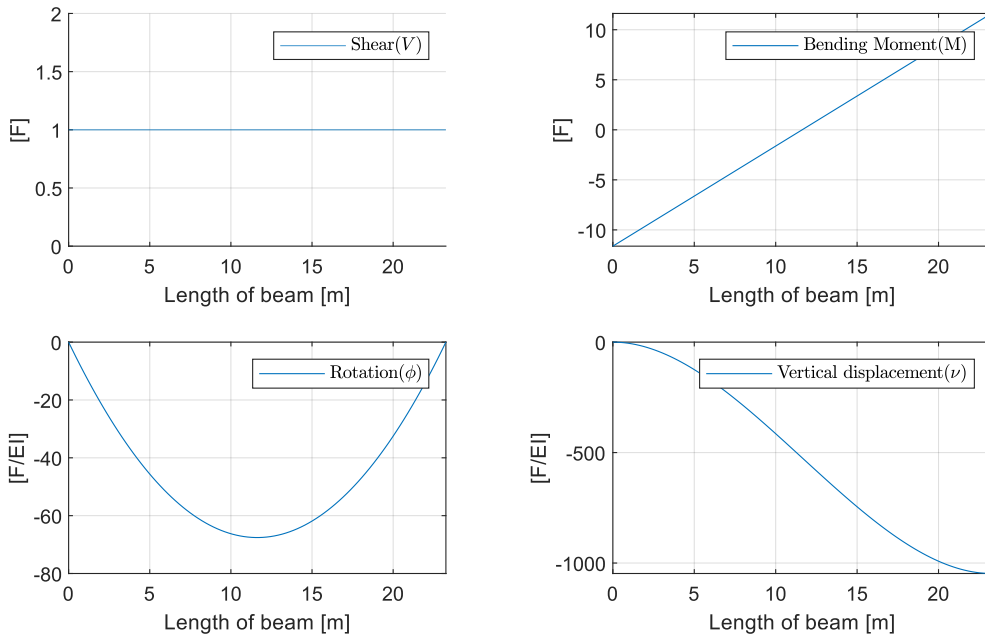


Figure 4.6: Response of a simple beam as a result of a vertical force applied to one end. The shear and bending moment are a function of the force. The rotation and vertical displacements are a function of the force over the Young's modulus and second moment of area.

The absolute displacement over the length of the beam,  $B$ , is determined next:

$$|\nu(B)| = \left| \frac{1}{EI} \left( \frac{1}{6} FB^3 - \frac{1}{4} FB^3 \right) \right| = \frac{FB^3}{12EI}$$

As the rotation is assumed small the absolute displacement is assumed equal to the length,  $x$ , times the angle  $\theta$  in radians. The maximum rotation of  $0.36^\circ$  defined as the stiffness criterion lies within this region of small angles. This makes it possible to determine the force  $F$ . The work done by this force,  $U_B$ , is determined next.

$$|\nu(B)| = dw = x \sin(\theta) \approx x\theta \quad (4.6)$$

$$F = \frac{12EIx\theta}{B^3} \quad (4.7)$$

$$U_B = F|\nu(B)| = \frac{12EIx^2\theta^2}{B^3} \quad (4.8)$$

The torque which is applied to the elements (torsion boxes and beams) is given by the following equation:

$$T = \frac{GJ\theta}{B} \quad (4.9)$$

The work done by the torque is given by the following equation:

$$U_T = T\theta = \frac{GJ\theta^2}{B} \quad (4.10)$$

Substitution of Equation 4.1 provides the angle of twist of the hulls  $\theta$ :

$$\theta = \frac{M_p}{\sum \frac{12E_i I_i x_i^2}{B^3} + \sum \frac{G_i J_i}{B}} \quad (4.11)$$

Where:

- $x_i$  : Longitudinal distance between the centre of a crossbeam and the global centre of twist defined below.
- $x_{CT}^*$  : Longitudinal distance between the datum and the centre of twist, defined below.
- $x_i^*$  : Longitudinal distance from an arbitrary datum to the neutral axis or the centre of twist of a crossbeam, in m.

$$x_{CT}^* = \frac{\sum \frac{12E_i I_i x_i^*}{B_{Bi}^3}}{\sum \frac{12E_i I_i}{B_{Bi}^3}}$$

$$x_i = x_i^* - x_{CT}^*$$

There are multiple methods to define the stiffness a certain shape has against rotation, called the torsion constant. This torsion constant,  $J$ , required for Equation 4.11 can be calculated by summing the second moments of area. This however, only holds for closed circular sections and is a large simplification for other shapes. To improve the model the torsion constant of the beams is calculated according to the equations given by Roark(1976)[22] which follows the Saint-Venant theory for open sections:

$$J = \frac{1}{3} \int_{sect} t^3 ds \quad (4.12)$$

Where:

- $t$  : thickness
- $s$  : surface

The I beams have a very low torsional constant as there are no closed sections, which are much more torsion stiff. The I beams have a maximal torsional constant of  $0.0002m^4$  for the given dimension range and so are negligibly small.

### Timoshenko - Ehrenfest beam theory

The Timoshenko - Ehrenfest beam theory does take into account the shear deformations. This method is better suited for thick beams and will have the same results for thin beams as the Euler - Bernoulli beam theory. The theory results in two relations that link the applied force and moment distribution to the responses:

$$M_y = -EI \frac{\partial \theta}{\partial y} \quad \text{and} \quad V_y = \kappa AG \left( -\theta + \frac{\partial \nu}{\partial y} \right) \quad (4.13)$$

Where:

$\kappa$  : Timoshenko shear coefficient, which depends on the geometry [6]

The boundary conditions remain equal to the conditions used for the Euler-Bernoulli theory. This also results in equal shear force and bending moment distributions.

Shear:

$$V(y) = F$$

Bending moment:

$$M(y) = \int V(y) dy = Fy - \frac{FB}{2}$$

Substituting these distributions in Equation 4.13 and implementing the boundary conditions gives the following results:

$$\theta(y) = \frac{Fy^2}{2EI} - \frac{FB y}{2EI} \quad (4.14)$$

$$\nu(y) = \frac{Fy^3}{6EI} - \frac{FB y^2}{4EI} - \frac{Fy}{\kappa AG} \quad (4.15)$$

The rotation is also equal to the rotation from the Euler theory. So for these boundary conditions, only the vertical displacement is affected by the Timoshenko theory. The final term in Equation 4.15 implements the shear deformation and is the only term that changes compared to the Euler-Bernoulli term.

### Stress in beam elements

With the angle of rotation known the individual forces and torsion moments per beam can be calculated. The maximum normal stress can be found by dividing the maximum bending moment over the section modulus. As can be seen from Equation 4.3 and in Figure 4.6 the bending moment is largest at both ends. So the maximum normal stress due to bending will occur in the ends, furthest away from the neutral axis.

$$M_{B,i} = F_i B_i / 2 \quad (4.16)$$

$$\sigma_i = M_{B,i} / SM_i \quad (4.17)$$

Where:

$B_i$  : Length of structure  $i$

$SM_i$  : Section modulus of structure  $i$

The shear stress,  $\tau$ , is a result of the constant shear force over the beams, shown in Figure 4.6. The shear stress is not equal over the cross-section of these beams. This is a result of the varying thickness over the beam as well as the first moment of area,  $S_x$ , which follows from Equation 4.18. The shear stress is largest in the centre and much smaller in the flanges.

$$\tau = \frac{V_y S_x}{I_x t} \quad (4.18)$$

Where:

- $V(y)$  : Shear force
- $S_x$  : First moment of area
- $I_x$  : Second moment of area
- $t$  : Thickness

The maximum shear stress in the cross-section of an I-beam occurs in the centre. The derivation of the equation for the maximum shear stress can be found in section A.2.

$$\tau_{max} = \frac{V(y)}{8I} \times \left[ \frac{B}{b} \times (H^2 - h^2) + h^2 \right] \quad (4.19)$$

The most critical point in the beams is where the combination of normal stress due to beam bending and the shear stress combination is largest. On the neutral line where the shear stress is largest, the normal stress is zero. In the flanges where the normal stress is largest, the shear stress is almost zero. Where the shear web connects to the flanges there is relatively high shear stress as well as normal stress. At the beam ends the bending moment and so the normal stress is largest. The shear stress is constant over the length of the beam. The connection between the flange and the web at the end of the beam is the most critical point, because of these effects. The shear stress at this critical point is determined in section A.2 and equal to:

$$\tau_{critical} = \frac{V(y)}{8I} \times \left[ \frac{B}{b} \times (H^2 - h^2) \right] \quad (4.20)$$

The normal stresses and shear stresses cannot be simply added as the yield criterion for shear stress is  $\sqrt{3}$  times lower than for normal stresses. The Von Mises yield criterion is used to check the combination of these stresses. The normal stresses and shear stresses are combined in an equivalent Von Mises stress, with the equation shown below.

$$\begin{aligned} \sigma_v &= \sqrt{\frac{(\sigma_{11} - \sigma_{22})^2 + (\sigma_{22} - \sigma_{33})^2 + (\sigma_{33} - \sigma_{11})^2 + 6(\sigma_{12}^2 + \sigma_{23}^2 + \sigma_{31}^2)}{2}} \\ &= \sqrt{\frac{(\sigma_n)^2 + 0 + (-\sigma_n)^2 + 6(\tau^2)}{2}} \end{aligned} \quad (4.21)$$

### Torsion box

The cross structure has a double hull which can be modelled as a row of hollow thin-walled rectangles, as indicated in Figure 4.2. These small torsion boxes and the indicated larger torsion box can be modelled with the following equation for the torsion constant[22]:

$$K = \frac{2tt_1(a-t)^2(b-t_1)^2}{at + bt_1 - t^2 - t_1^2} \quad (4.22)$$

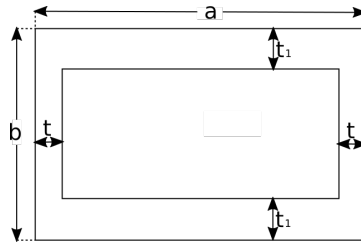
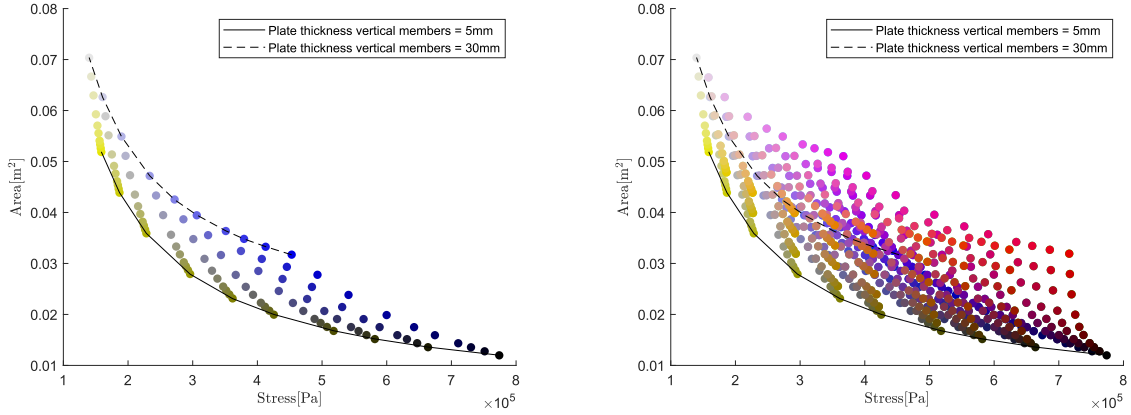


Figure 4.7: Dimensions for Equation 4.22[22]

The bottom of the cross-deck is modelled as a wet deck and a dry deck with a certain height between them. The length is divided into several squares. To maximize the torsion constant the width of the torsion boxes,  $a$ , is kept as close as possible to the height,  $b$ , see Figure 4.7 and Equation 4.22. The plate thickness can now be varied. The wet deck and dry deck are kept at the same plate thickness,  $t_1$ ,

while the individual horizontal plates have a thickness of  $t \cdot 2$ . The highest stress occurs as a result of bending in the outer parts of the structure. This stress is plotted over the section area, see Figure 4.8a. In this figure, the plate thickness of both decks,  $t_1$ , is varied as well as the thickness of the vertical members. The most optimum data points lay in the lower-left corner of the figure, where the stress is lowest as well as the used material, measured in area. In Figure 4.8b the thickness of both decks, wet deck and dry deck are varied separately as well. This does not result in more optimal data points as expected from Equation 4.22. From Figure 4.8 can be concluded that it is optimal to have the vertical members as thin as possible. This is a result of the very low torsion constant of these torsion boxes. The individual torsion boxes absorb more energy in bending. When the distance between the centre of twist and the torsion box increases this effect increases. Because the individual torsion boxes are loaded by bending the vertical members do not absorb as much energy as the horizontal (deck) members.



(a) Varying plate thickness of vertical structures and decks. (b) Varying plate thickness of vertical structures and both decks separately.

Figure 4.8

### Bredt's theory

The torsion constant as a result of Equation 4.22 does not include the interaction between the different boxes. To include these interactions Bredt's theory can be used. Bredt's theory assumes constant stress over the thickness. The multiple individual torsion boxes between the wet and dry deck are coupled into one multi-cell of torsion boxes. The torsion constant for free warping,  $I_p$ , can be calculated according to the following equation:

$$I_p = 4\{\Omega\}^T [S]^{-1} \{\Omega\} \quad (4.23)$$

Where:

- $\Omega$  : closed-cell area vector
- $S$  : contour matrix

When the moment applies in the centre of the multi-cell the torsion boxes do not react to bending and only to pure torsion. Because the box shape is not circular distortion will occur. Due to the torsion, there will be a displacement in the direction of the beam, called warping. This warping,  $u$ , is varying over the surface,  $s$ . The torsion box (multi-cell) is assumed to have a free warping condition because the demi-hulls where they are fixated to, have a low stiffness in the transverse direction.

$$u(s) = \frac{1}{G} \int_s \frac{q_i}{t_p(s)} ds - \theta \int_s \rho(s) ds + C \quad (4.24)$$

Where:

- $q_i$  : shear flow in cell  $i$
- $t_p$  : plate thickness

$$u(s) = \theta \cdot \omega(s) \quad (4.25)$$

Where:

$\omega(s)$  : sectorial coordinate distribution over the surface

This sectorial coordinate distribution can be found with the equations shown below. The constant,  $C$ , is found in a step-by-step process starting on a symmetry axis where the warping and the sectorial coordinate distribution are known and equal to zero. The equations for a thin-walled cell and for a multi-cell are slightly different.

Closed thin-walled cell:

$$\omega(s) = - \int_s \rho(s) ds + 2\Omega \frac{\int_s \frac{1}{t_p(s)} ds}{\oint \frac{1}{t_p(s)} ds} + C \quad (4.26)$$

Multi-cell:

$$\omega(s) = - \int_s \rho(s) ds + \frac{1}{\theta G} \int_s \frac{q_i}{t_p(s)} ds + C \quad (4.27)$$

The stress in the torsion box(es) is pure shear stress, no normal stresses are present due to the free warping condition. The shear stress is a result of the shear flow,  $q$ , which goes around in each cell. On the plane, where two cells are combined in a multi-cell, the shear flows are opposite in direction and counteract each other, as depicted in Figure 4.9. Due to this the shear flow and so the shear stress are largest on the outer plates.

$$\{q\} = \frac{M_t}{2} \cdot \frac{[S]^{-1}\{\Omega\}}{\{\Omega\}^T [S]^{-1}\{\Omega\}} \quad (4.28)$$

Bredt's theory assumes that the stress is equal over the thickness of the plate. The shear stress is determined with the following equation:

$$\tau = \frac{q}{t} \quad (4.29)$$

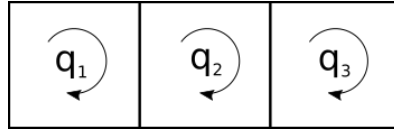
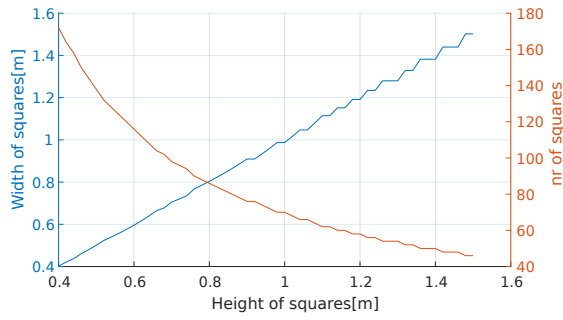


Figure 4.9: The shear flow that goes round in each cell and counteracts at the shared planes

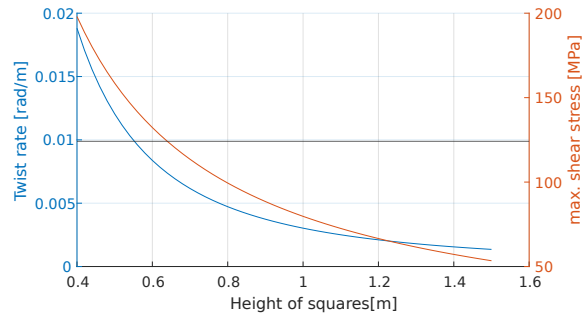
### Effectiveness of torsion

In order to find the most effective design of the double bottom with torsion boxes, an analysis is performed. The multicell equations determined by Bredt's theory are used. In Figure 4.10 the results can be seen when the height of the torsion boxes is increased. The width of the torsion boxes is kept as close to the height to keep them as square as possible. Increasing the height and the width of the torsion boxes results in a higher torsion constant,  $I_p$ , and a lower twist rate. The maximum shear stress is also lowered. In Figure 4.10b the vertical line resembles the yield stress for shear. The effectiveness of the structure is measured by the torsion constant divided by the material needed, expressed in area. Because the area of the complete structure keeps quite constant over the change in height while the stiffness increases significantly the effectiveness of the structure goes up for a larger height. Unfortunately, the height of the double bottom is limited to 0.6m. At this length, the maximum stress exceeds the yield stress for shear.

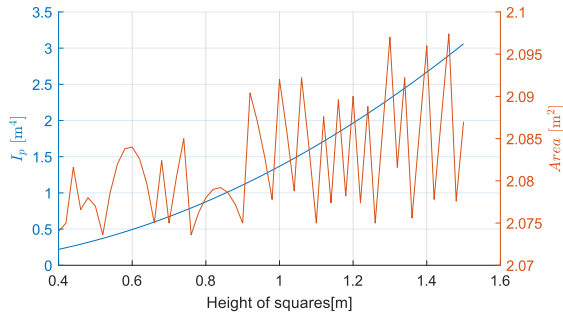
When the height of the boxes is set at the most effective value possible of 0.6m, the number of individual boxes can still be varied. This analysis is done and the results can be seen in Figure 4.11. Changing the number of squares results in a relatively small decrease in twist rate and shear stress. The torsion constant shows only a small positive effect by increasing the number of squares. However, this increase is only small while the area increases much more. As a result of this, the effectiveness of the structure decreases with an increasing amount of cells. The most optimal situation has the least amount of cells according to this analytical analysis.



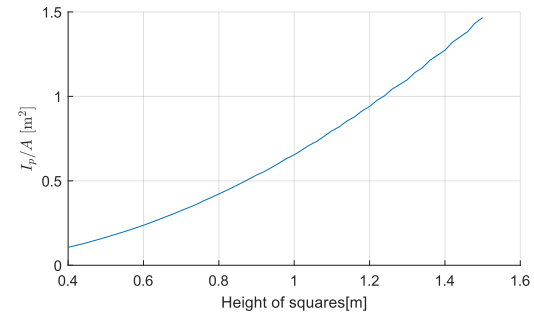
(a) Torsion box length and number of cells over the torsion box height



(b) Rate of twist and max. shear stress over the torsion box height

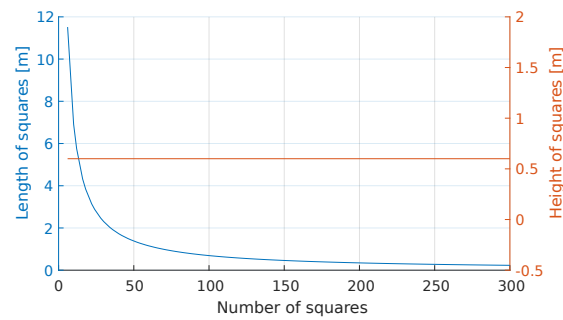


(c) Multi-cell free warping torsional stiffness,  $I_p$ , and the multi-cell area over the torsion box height

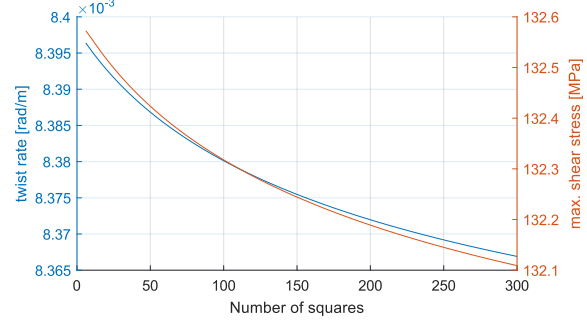


(d) Multi-cell free warping torsional stiffness,  $I_p$ , divided by the area over the torsion box height

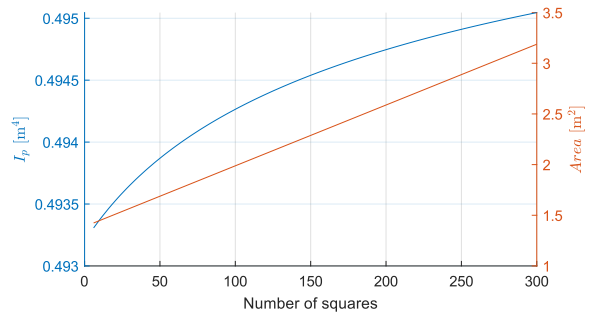
Figure 4.10: The multi-cell torsional element with square boxes from 10mm aluminium, varying the height as well as the individual length to keep the cells as square as possible.



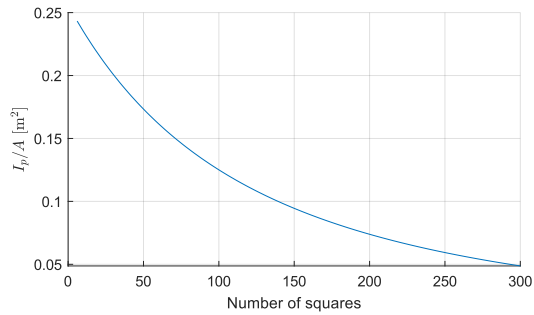
(a) Torsion box length and height of cells over the number of cells



(b) Rate of twist and max. shear stress over the number of cells



(c) Multi-cell free warping torsional stiffness,  $I_p$ , and the multi-cell area over the number of cells



(d) Multi-cell free warping torsional stiffness,  $I_p$ , divided by the area over the number of cells

Figure 4.11: The multi-cell torsional element with a constant height and varying length due to the varying amount of cells

## Weight optimization

In this section, multiple configurations, based on the transverse structure design shown in Figure 4.2, are analyzed.

The first design includes all 4 beams at 34, 49, 59 and 82m aft. The flanges have a width of 1.5m and the total height of the beams is 3.4m. In order to comply with the stiffness criterion, the rotation over the length of the beams, the centreline separation length, should not exceed  $0.26^\circ$ . This limitation is met by making the beams with a minimum constant plate thickness of 27mm. This thickness is not available but is used to show the difference. The cross sections have a total area of  $0.69\text{m}^2$ .

The transverse structure can also just use the most fore and aft beam and neglect the central two. To satisfy the criterion a minimum plate thickness of 28mm is required. This results in an area of  $0.36\text{m}^2$  which is of course much less than using all four beams. This makes this design more effective.

The two middle bulkheads and the decks in between can however be modelled as a large torsion box of  $3.6 \times 10\text{m}$ . Modelling both outer I-beams and the large torsion box with an equal constant plate thickness of 22mm results in a model that satisfies the criterion. However, the area of both beams and the box is  $0.58\text{m}^2$ .

This shows that the most effective design does not use the central bulkheads as I-beams, this is very ineffective. Modelling these beams and the decks that lay in between, as one large torsion box is more effective. The design that does not use torsion boxes and only focuses on the most fore and aft beam is however the most effective. This design can be further optimised. The thickness of the shear web can be decreased as the flanges are most important. When the shear web is given a thickness of 10mm and both flanges a thickness of 40mm the construction becomes stiffer while the area drops to  $0.3\text{m}^2$ . This area results in a total weight of 19 tonnes for both beams, which is 13% of the weight from the bare hull as determined in section 4.1. To further optimize this set up the design of the flanges could vary over the length of the beam, or the width of the ship. Because the bending moment is largest at both ends while in the centre the bending moment is equal to zero and smaller flanges would suffice.

## 4.2.2 Finite element analysis

In this section, the beam bending theory, derived in the previous section, will be compared with a finite element (FE) analysis. The same is done for the analytical theory of the torsion boxes. The FE analysis of a bending I-beam will then be improved by integrating more realistic boundary conditions. A more complex I-beam is designed that will fit in the current design of the vessel. This complex I-beam is analyzed with the analytical method and the finite element method.

### Beam bending

A single I beam with the dimensions given in Table 4.1 is examined. The beam has a vertical force and a fixed rotation applied to one end while the other end is fully fixed. The length of the beam is assumed equal to the centre line separation,  $s$ , of 23.25m to provide room within the hulls (4m on both sides) for the clamping of these beams in the demi-hulls.

Table 4.1: Dimensions of I beam, see Figure 4.12

$B_1$	1700 mm	$T_1$	30 mm
$B_2$	1700 mm	$T_2$	30 mm
H	3400 mm	b	10 mm

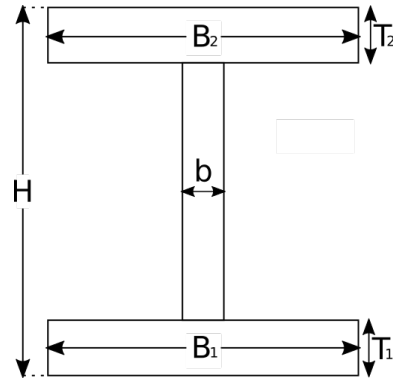


Figure 4.12: I beam dimensioning

The vertical displacement of this beam under the applied force is acquired from both the analytical model and a beam element in the finite element (FE) software Strand7. The normal stress, shear stress and Von Mises stress from the analytical model are also checked with the result from the FE analysis. These stresses are shown in Figure A.2

In Figure 4.14a and Table 4.2 it can be seen that the normal stress,  $\sigma_n$ , complies very well with the FE analysis. The maximum shear stress,  $\tau_{max}$ , calculated with Equation 4.18 also complies very well. However, in Figure 4.14b it can be seen that the shear stress is not equal over the cross-section. The shear distribution function used to calculate the shear in the most critical corners does not take into account such a large deviation. This is due to the relatively thin shear web. The analytical method to define the shear force distribution over the cross-section results in only a slight change between the maximum shear stress in the centre and the shear stress in the critical point. The FE analysis shows a larger change in shear stress, see Table 4.3. The Von Mises equivalent stress is largest near the corners where it exceeds the 300MPa scale. With the analytical method of determining the shear stress, the shear stress is expected too large on the top and bottom of the web. This results in a larger maximum Von Mises stress in the corners of the web.

Table 4.2: Stress results of beam theory and finite element analysis with and without taking into account the shear areas of the beam

	Applied force:	Max. vertical displacement:	Max. shear stress:	Max. normal stress:
<b>Euler-Bernoulli beam theory:</b>	4661 kN	217 mm	145 MPa	287 MPa
<b>FEA (no shear area):</b>	4661 kN	217 mm	145 MPa	287 MPa
<b>Timoshenko beam theory:</b>	4661 kN	413 mm	145 MPa	287 MPa
<b>FEA (incl. shear area):</b>	4661 kN	342 mm	145 MPa	287 MPa

Table 4.3: Stress results of Euler-Bernoulli beam theory and finite element analysis in the critical point on the connection between the shear web and flange

	Applied force:	Max. vertical displacement:	Crit. shear stress:	Crit. normal stress:	Max. Von Mises stress:
<b>Beam theory:</b>	4661 kN	217 mm	125 MPa	282 MPa	360 MPa
<b>FEA:</b>	4661 kN	217 mm	72 MPa	282 MPa	314 MPa

The Euler-Bernoulli beam theory does not include the shear deformation. The FE analysis provides an option to not take the shear areas into account, to eliminate shear deformations. The vertical displacement and so the stiffness of the beams is identical for both models that eliminate the shear deformations, as can be seen in Table 4.2. When the FE analysis does take the shear areas, and so the shear deformation into account the deformation enlarges, so the structure becomes less stiff. The Timoshenko beam theory also takes into account the shear deformation. The Timoshenko beam theory overestimates the deformation as a result of shear. The vertical displacement is 20% larger than the vertical displacement determined by the FE analysis as can be seen in Table 4.2 and Figure 4.13. Both the vertical shear away from the centre as well as the shear deformation are overestimated.

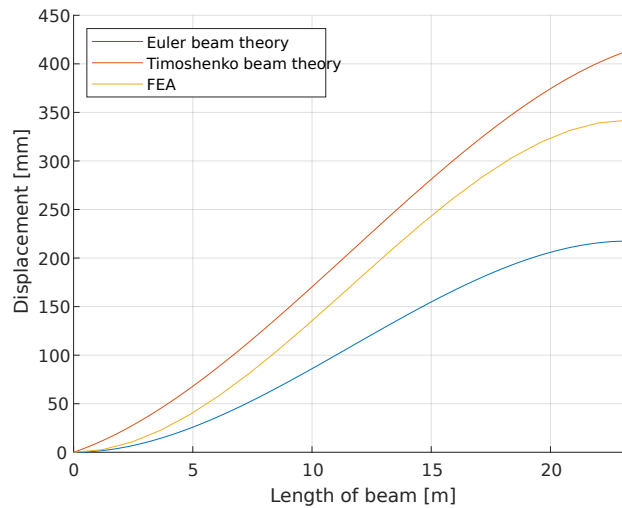
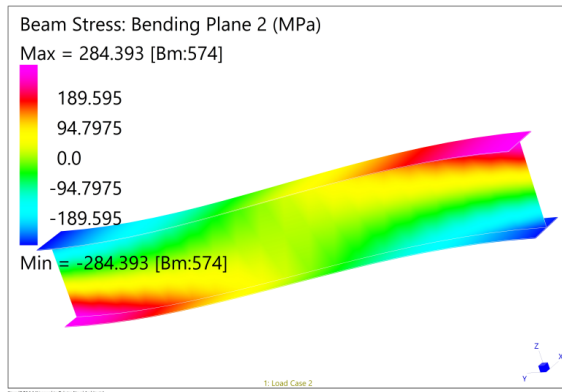
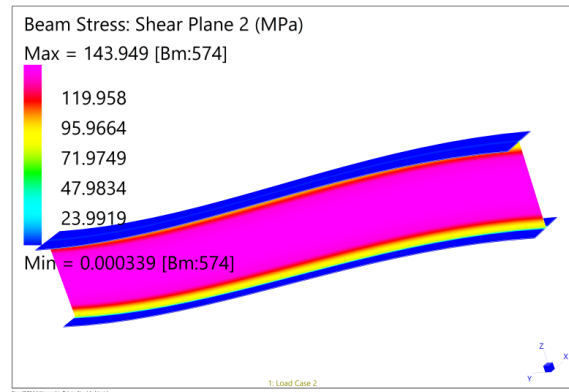


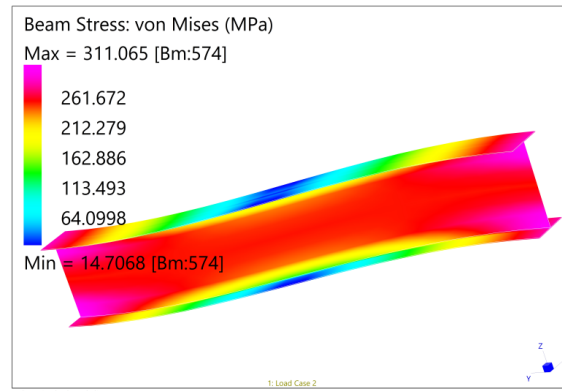
Figure 4.13: Vertical displacement over the length of beam



(a) Normal stress



(b) Shear stress



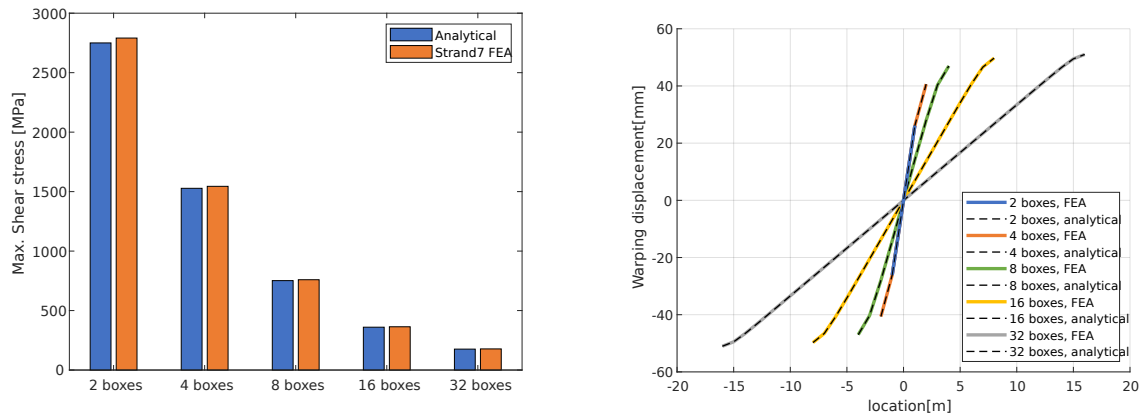
(c) Von mises stress

Figure 4.14: Stress in simple I beam

### Torsion box

The results from Equation 4.23 with Bredt's theory have been compared with the results from FEA software Strand7. This is done for multiple multi-cells with a varying number of boxes. Each box has dimensions of 1 by 1m and is modelled as aluminium. The free warping displacement according to Bredt's theory assumes constant shear stress over the thickness and is only valid for small thicknesses, a thickness of 10mm is used in the analysis. The torsional moment of 110000kNm was applied in the centre and was in the FE analysis distributed by a 'spider' of solid links. The length of the multi-cell was 1m, so the angular displacement over the length is equal to the rate of twist.

The analytical analysis resulted in the free warping displacements over the width of the multi-cell as shown in Figure 4.15b by the dashed lines. The free warping displacement calculated by the FE analysis is equal. The maximum shear stress, which occurs in the centre of the top and lower plate is equal in both methods, see Figure 4.15a. The results from the FE analysis are shown in Figure 4.16. The rotation, max. warping displacement and max. shear stress are also given in Table 4.4. In this table it is shown that the results from the analytical model are (almost) equal to the results from the FE analysis. The largest deviation occurs for the shear stress. This is the result of the difference in shear stress over the thickness of the plate, which is neglected in the analytical model. The shear stress on the centreline of the plate determined by the FE analysis is equal to the shear stress determined by Bredt's theory.



(a) Maximum shear stress,  $\tau$ , for the analytical and FEA model. (b) The free warping displacement along the top of the boxes. Upper left corner negative displacement. Upper right corner positive displacement.

Figure 4.15

Table 4.4: Results from analytical and FE analysis of multi-cells consisting of cells of 1x1m.

	Rotation [deg]					Max. warping disp. [m]				
	2-box	4-box	8-box	16-box	32-box	2-box	4-box	8-box	16-box	32-box
Analytical	8.984	3.661	1.650	0.785	0.384	26.1	40.6	47.0	49.7	51.0
FE analysis	8.980	3.659	1.648	0.784	0.383	26.1	40.6	47.0	49.7	51.0
	0.0%	-0.1%	-0.2%	-0.1%	-0.2%	0.0%	0.0%	0.0%	0.0%	0.0%

	Max shear stress [MPa]				
	2-box	4-box	8-box	16-box	32-box
Analytical	2750	1528	751.8	360.2	175.9
FE analysis	2791	1544	759.3	363.8	177.6
	1.5%	1.1%	1.0%	1.0%	1.0%

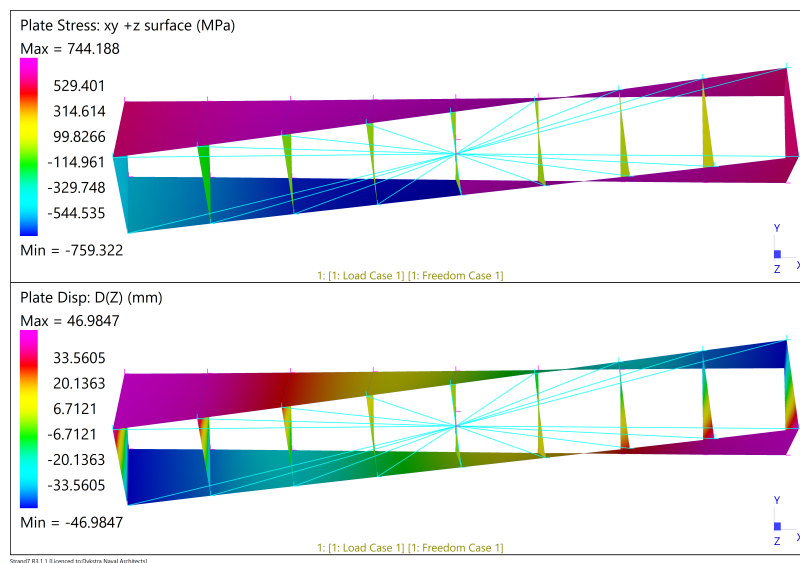


Figure 4.16: FEA of multi-cell with 8 torsion boxes, top = shear stress, bottom = warping displacement

When the warping of the torsion boxes is constrained different results are expected. When the warping is completely constrained, so no warping is allowed the shear flow does not go round in each cell. Instead, the vertical elements are vertically loaded and deformed by shear. The top and bottom elements in the constrained model do not absorb much energy as can be seen from the stress results in Figure 4.17. All stress is in the vertical members. By limiting the warping the structure becomes much stiffer. The rotation for both the constrained warping and free warping model are shown in Figure 4.18. The rotation of the constrained warping model is 77% smaller than the model with free warping. So, the stiffness is increased by 77% for this set-up by constraining the warping displacement.

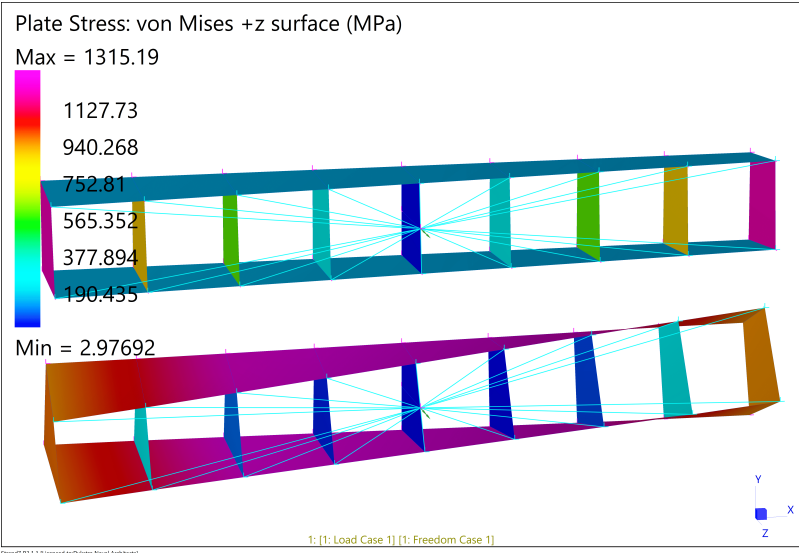


Figure 4.17: FEA of multi-cell with 8 torsion boxes Von Mises stress, top = constrained warping, bottom = free warping

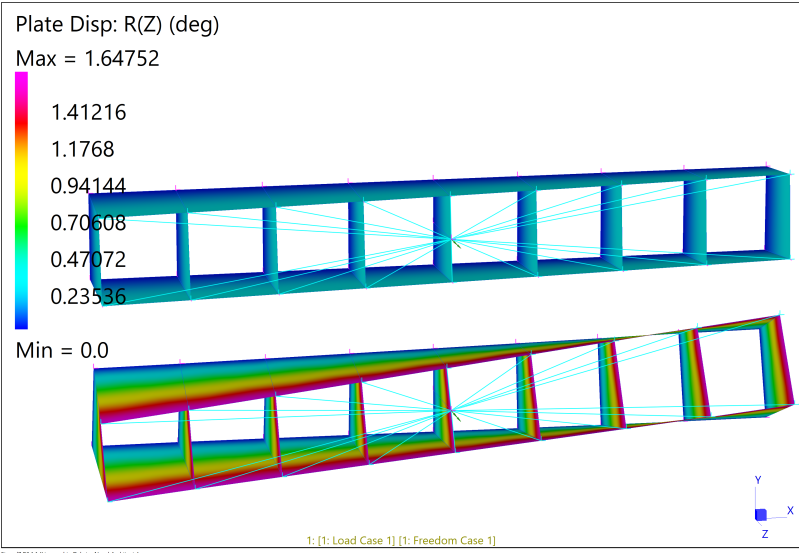


Figure 4.18: FEA of multi-cell with 8 torsion boxes rotation, top = constrained warping, bottom = free warping

## Optimization of the FE analysis

The flanges of the I beams are the decks that may be locally stiffened. The width of these 'flanges' is critical in the bending stiffness of these beams. The width of the flanges can not be equal to the width of the whole deck. The failure mode of I beams with a large width to thickness ratios in the flanges is local buckling of the beam flange citeIguchi2002EffectsRoot.

The bending stress in the flanges is highest near the web. The bending stresses in wide flanges decrease over the distance from the web. This phenomenon is called shear lag or stress diffusion[17]. The effective breadth methodology by Schade (1951) has been proven effective to model this effect. As shown in Figure 4.19 the shear distribution over the flange is modelled with an effective breadth at the maximum stress,  $\sigma_{max}$ . The integral of the stress over the breadth is kept constant. However, this method requires a stress distribution over the full plating which is not available. Tigkas et al. (2011) researched the effective breadth of 29 simple structures, made of a plate with a stiffener. They developed a uniform rule for the effective breadth depending on the maximum breadth and length of the beam, see Equation 4.30[12]. The actual breadth,  $b$ , required in Equation 4.30, is not available. For this problem of finding the width of the flanges, a different solution is needed.

$$\frac{b_{eff}}{b} = \left(1 - e^{-0.4l/b}\right) \quad (4.30)$$

Where:

- $b_{eff}$  : Effective breadth of the flange
- $b$  : Actual breadth of the flange
- $l$  : Length of the beam

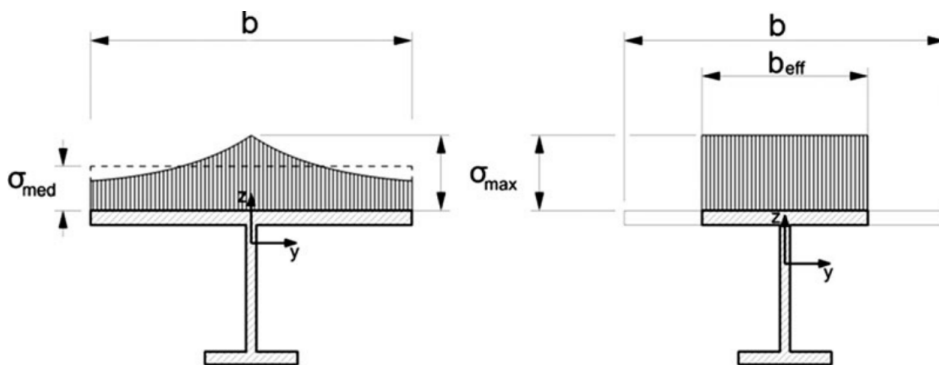


Figure 4.19: Effective breadth definition with the actual and fictitious bending stress distributions[10]

A beam element with wide flanges is modelled in a finite element analysis with 200,000+ 3d elements (tetra4). A vertical load is applied to the shear web on one end of the beam and a counteracting load is applied to the other end. The rotations are fixed at the full beam end. This results in the s-curve deflection, shown in Figure 4.20. This figure also shows the normal (compression/tension) stresses. From Figure 4.20 can be concluded that where the moment is largest, at both beam ends, the flanges do not contribute with unlimited width. In the previous FE analysis the normal stress over the breadth of the flange is constant, see Figure 4.14a. The difference between both analyses is the location where the load is applied. Applying the vertical load only to the shear web is a more realistic situation, as the bulkheads in both demi-hulls are much stiffer in the vertical direction than the decks.

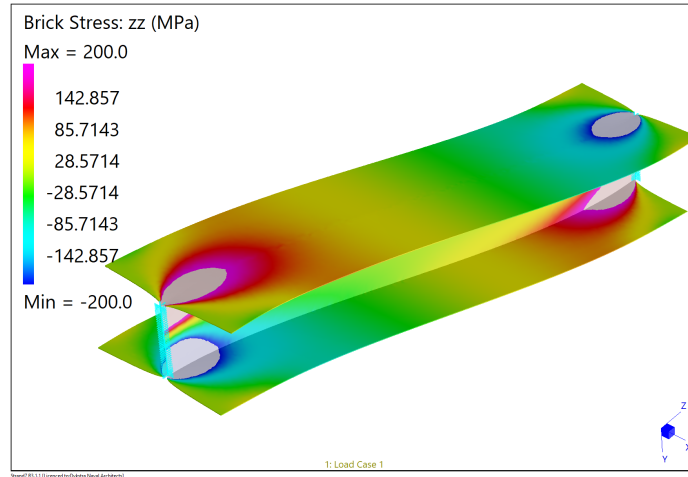
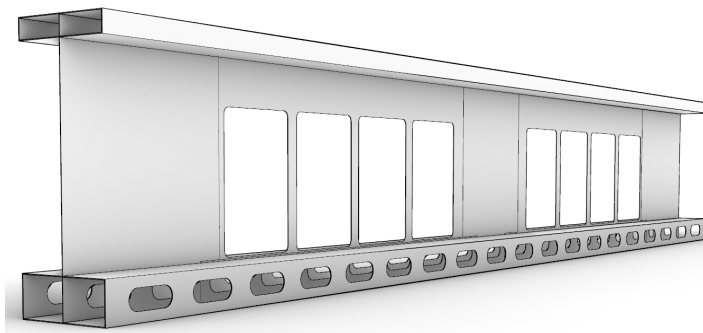


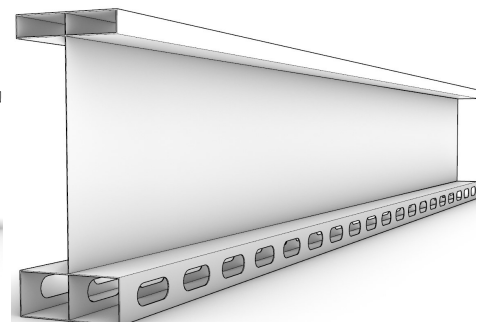
Figure 4.20: Axial stress in I beam with boundaries applied to the shear web. 25m long, 5.5m wide, 3m high and plate thickness of 30mm

### Complex beam design

In order to optimize the use of the flange, the vertical load should be applied to the flange in the best way possible. To arrange this, the width of the flange is set to be twice the frame spacing. The load can then be applied to the centre by the bulkhead/shear web and also on the sides by the frame. All vertical members drawn in black in Figure 4.22 are loaded. Keeping the flange between the frame spacing gives a flange width of 1.5m. When the thickness of the flange is above 37mm this flange width complies with the rule established by Lambert (1968). This rule says that the width should not exceed 40 times the thickness of the flange[15]. In order to make the flanges easier manufacturable and to prevent buckling in the compression flange, one flange is split into two flanges and two vertical elements creating a box structure as can be seen in Figure 4.22. The lower box-like flange lies between the dry deck and wet deck. All sorts of connections need to pass through this section, like plumbing, electricity, etc. This is accommodated for by openings in the vertical members. The forward beam is drawn in Figure 4.21b. The aft beam has large additional holes in the shear web to accommodate for the sliding doors located in the aft. The aft beam is drawn in Figure 4.21a.



(a) Drawing of aft I-beam configuration



(b) Drawing of forward I-beam configuration

Figure 4.21

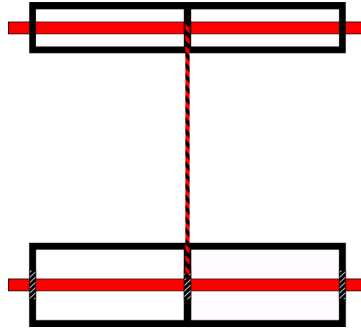


Figure 4.22: The complex design of the beams in black, the black and white dashed areas indicate the holes in the shear web, in red the simplified beam is drawn, the shear web is shortened and not displayed at scale

These complex beam designs are analyzed. The overall pitch connecting moment is equal to 110000kNm, see section 3.3. The centre of twist lays in between both beams, resulting in a distance of 23.6m between the beam and the centre of twist. On each of the beams, a positive or negative vertical force of 4660kN is applied to account for the pitch connecting moment.

The complex beam design is simplified for the analytical model. Both top and lower flanges are combined into two flanges laying in the middle of the 'box', drawn in red in Figure 4.22. The area of the vertical members in the flange is only compensated for by 50% as they have holes. This gives the flange a thickness of twice the thickness in the complex design. The width of the flange in the analytical model is 1.7m instead of the 1.5m in the complex design. The height of the I-beam is 3.4m. The yield strength of aluminium of 215MPa is lowered by 30% to accommodate for local loads. This leaves a maximum normal stress of 150MPa and a maximum shear stress of 87MPa, as the material in yield is  $\sqrt{3}$  times weaker. When the simplified flanges have a thickness of 70mm the maximum normal stress is 144MPa. When the shear web is given a thickness of 20mm the maximum shear stress is 73MPa. For such beam, the vertical displacement is equal to 109mm which gives a rotation of  $0.13^\circ$ . These beams fulfil both the stress and stiffness criteria.

The sail loads can be added to this analytical beam to see what the result is on the stress. The moment is equal to 17108kNm divided by two. The maximum bending moment in the beam ends is equal to 54184kNm, so the increase by the sail load is 16%. The maximum normal stress on one side of the beam is increased to 167MPa while it lowers on the other end. The side force,  $F_y$ , as a result of the rigging results in another small increase in the normal force of 3MPa.

When the complex design is modelled in Strand7 with a thickness of 35mm in the complex flange and 20mm in the shear web the results vary much from the analytical model. The results are shown in Figure 4.23 and Figure 4.24. In these figures, the normal stress, as well as the Von Mises stress, is limited because the application of the load on only the vertical members results in high-stress concentration. The required cut-outs in the vertical members also result in large stress concentrations.

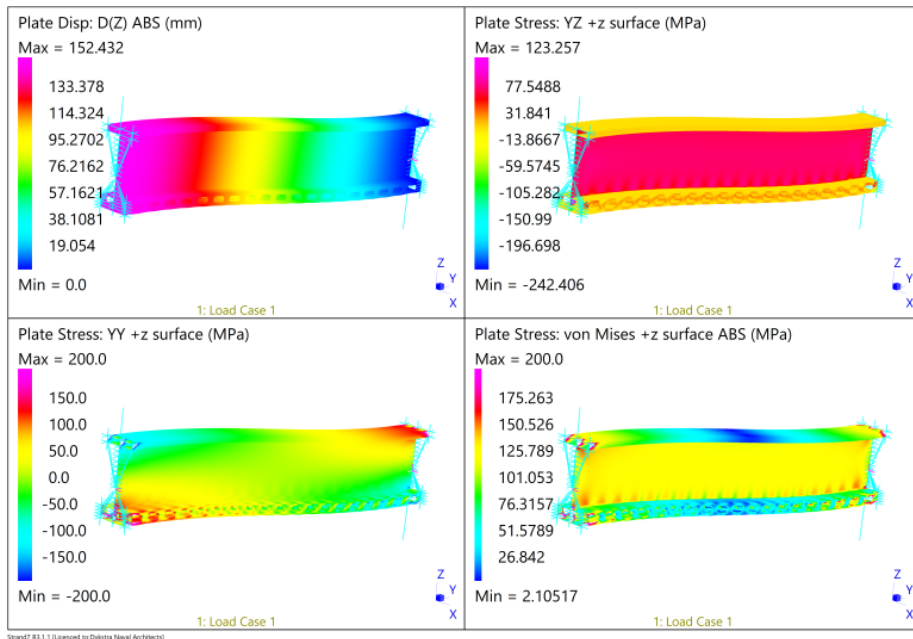


Figure 4.23: FE analysis of the forward beam

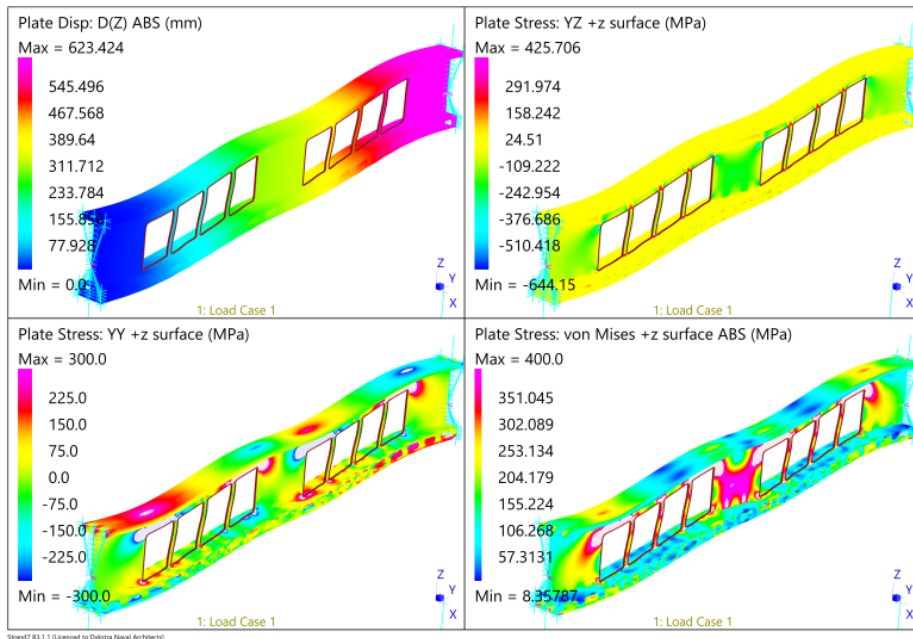


Figure 4.24: FE analysis of the aft beam

### 4.3 Conclusion

The response of the vessel loaded in head seas condition is analyzed in the same way as for monohulls. The cross-section of the vessel is simplified to determine the most critical stress. This is a normal stress as a result of the longitudinal bending moment. Due to the slender and high hull shapes of both demi-hulls, it is relatively easy to keep the stresses within their limitations.

The torsional moment as a result of the quartering waves is analysed with an analytical beam model. The transverse structure is not only stress driven but the stiffness is also of importance to keep the

superstructure from breaking. The maximum rotation over the centreline separation distance is  $0.26^\circ$ . The analytical beam model is compared with an FE analysis and shows equal results on the maximum normal and shear stresses. However, the shear distribution over the shear web shows a large deviation between the two. The analytical method results in a larger shear stress in the connection point with the flange. This results in an overpredicted Von Mises stress in the analytical model as well as an overpredicted deflection, when the shear deflections are taken into account.

Torsion boxes as part of a multi-cell are analysed as well and they show equal results as the FE analysis. The shear stress varies only a small amount because the analytical model assumes a constant shear stress over the thickness of the plate. From the analytical model can be concluded that the torsion boxes are less effective than a structure that includes beams. This is a result of the large arms the beams can have to the centre of twist.

The FE analysis is optimized by only loading the I-beam in the vertical elements. The design is also made more complex due to required cut-outs in the shear web. These complex beams do not follow the analytical model any longer and no predictions on the response of these complex beams can be made without the use of FE analysis. Due to the complexity of the beams the analytical method is not useful in the design of these beams. However the analytical method has shown value by indicating the value of torsion boxes compared to beams.

The head sea loading condition is less complex than the quartering sea loading condition and easier to solve. This makes the pitch connecting moment the dominant load. However for the longitudinal hull girder design the longitudinal bending moment is dominant. The additional sail loads result in an increase in the maximum stress in the beams of 16%.

# 5 | Evaluation

## 5.1 Conclusion

The design of large sailing catamarans starts with determining the overall dimensions. The loads can be determined when these are set, and a hull shape is known. This is done with the static wave method in a particular sea state. In head seas, the class societies give a good approximation compared to the static wave method. In quartering waves, the pitch connecting moment determined with the static wave approach complies with one class society, BV. This society uses wave height and length to determine the load. Other class societies do not make use of any dimension of the beam or hull separation, and these rules have a resulting moment which is three times larger. During the concept design phase, the static wave method is helpful as the class society might not be determined yet. Many parameters needed for acquiring the results from the class rules are not set either. A tool that defines the load based on first principles gives the engineer more insight into the actual problem. It might also be used next to the rules when working on a project that lays outside or on the border of the regular scope of the rules. The rules are still a deterministic process based on earlier builds and might give the wrong results.

The analysis of the longitudinal structure of the catamaran remains equal to the analysis of a mono-hull. Due to a catamaran's high and slender hulls, the longitudinal bending moment is not much of a problem. The pitch connecting moment is the dominant load case for the transverse structure. This torsional moment is a result of the quartering waves. In order to keep the superstructure from breaking, a stiffness criterion is defined by reversed engineering. The rotation of the demi-hulls is limited to  $0.26^\circ$  over the centreline separation distance. An energy model is used to determine the stiffness required to comply with this criterion. The energy model with simple beam theory is checked with FE analysis and shows great resemblance for the torsion boxes as well as for simple beams. The shear stress is due to the relatively narrow profile of the shear web over predicted analytically. This also results in a lower stiffness (-20%) beam according to the Timoshenko beam theory compared to the FE analysis. Using the beam theory, a design containing two I-beams is proposed. The design of these beams was strength driven as the stiffness requirement was met before the maximum stress requirement.

When more complex beams are used, especially with substantial holes, the analytical beam theory is not adequate anymore. Therefore, a more complex FE analysis of the single beam is required to find the right stiffness of the design with holes. This stiffness should be equal to the stiffness which follows from the energy model; Otherwise, the displacement will become too large.

## 5.2 Discussion

The static wave model for defining the wave-induced loads in both head and quartering seas does not incorporate any dynamic wave elements, like slamming. For this reason, the used wave height is rather conservative. This wave height can be lowered when dynamic effects are taken into account.

In the energy model as well as the FE analysis, the ends of the beam are fixed for the transverse displacement. However, both semi-hulls will not be infinitely stiff against longitudinal torsion, as assumed in this research. This will result in smaller bending moments at the beam ends, resulting in lower stresses. However, this will also increase the displacement of both hulls as well as the superstructure and make the structure less stiff. When the bending moments, as well as the resulting stresses, are lower, the plate thickness can be brought down. This will make the structure less stiff and make the stiffness criteria more important.

Both the analytical and FE analyses do not include a buckling analysis. The most optimal torsion boxes are large and thin, according to the analytical theory. However, these torsion boxes are also most likely to buckle.

The compression flanges of the I-beams are also prone to buckling. For the longitudinal structure as

well as the transverse structure, fatigue is not taken into consideration. Because the structure is made of aluminium, the structure might need to be larger to accommodate for fatigue. Aluminium does not have a fatigue limit. The aluminium will eventually always fail after a number of stress cycles, even for small stresses. However, small stress amplitudes will increase the number of cycles the material can withstand.

### 5.3 Recommendations

The rules for the pitch connecting moment by some classification societies could be improved by implementing the missing dimensions of the beam and float separation as the pitch connecting moment is based on these dimensions according to first principles. Further research could also improve the static wave method by finding and implementing a parameter for the dynamic effects of a wave, i.e. impact loads and accelerations. This could possibly lower the assumed wave height to length ratio and result in less conservative load cases. Where both demi-hulls are in this research assumed infinite stiff further research can implement the actual stiffness of both hulls and find the effect of these changing boundary conditions on the stresses and displacements. Research containing reverse engineering could find more correct conditions on the limitations of warping. When the torsion boxes are constrained in their warping, they become much stiffer and might become more effective against torsion than beams at this scale.

# A | Derivations

## A.1 Timoshenko shear coefficient

The Timoshenko shear coefficient which is a parameter in the Timoshenko beam theory is developed by Cowper (1966)[6] for various geometries. The equation for the shear coefficient of a symmetrical I-beam is given below. The required dimensions are shown in Figure A.1.

$$\kappa = \frac{10(1 + \nu)(1 + 3m)^2}{(12 + 72m + 150m^2 + 90m^3) + \nu(11 + 66m + 135m^2 + 90m^3) + 30n^2(m + m^2) + 5\nu n^2(8m + 9m^2)} \quad (\text{A.1})$$

[6]

Where:

$$\begin{aligned} m &= 2bt_F/ht_w \\ n &= b/h \end{aligned}$$

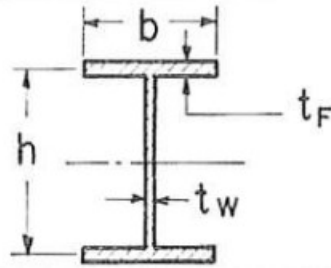


Figure A.1: Dimensions used for the Timoshenko shear coefficient developed by Cowper(1966)[6]

## A.2 Shear distribution I beam

The shear distribution is calculated separately for the flange and for the web. The derivation is shown below for the flange, which has a thickness,  $t$ , which is equal to the width of the flange,  $B$ . For this derivation horizontal and vertical symmetry are assumed. The dimensions used for this derivation can be seen in Figure A.2b.

$$q = \frac{V_y S_x}{I_x} \quad (\text{A.2})$$

$$\tau = \frac{q}{t} \quad (\text{A.3})$$

Where:

- $q$  : Shear flow
- $V_y$  : Shear force
- $S_x$  : First moment of area
- $I_x$  : Second moment of area
- $t$  : Thickness

$$S_x = A \cdot \bar{z} \quad (\text{A.4})$$

$$A = B \cdot \left( \frac{H}{2} - z \right) \quad (\text{A.5})$$

$$\bar{z} = z + \frac{1}{2} \left( \frac{H}{2} - z \right) = \frac{z}{2} + \frac{H}{4} \quad (\text{A.6})$$

$$\tau_{flange} = \frac{V_y}{I_x} \cdot \frac{B}{B} \cdot \left( \frac{H}{2} - z \right) \left( \frac{z}{2} + \frac{H}{4} \right) = \frac{V_y}{I_x} \left( \frac{H^2}{8} - \frac{z^2}{2} \right) \quad (\text{A.7})$$

For the top of the upper flange  $z = H/2$ , so the shear stress is zero. The maximum shear stress in the flange occurs on the lower side of the upper flange and the top side of the lower flange, as can be seen in Figure A.2a. Here  $z$  is equal to  $h/2$  which results in the following shear stress:

$$\tau_{flange,max} = \frac{V_y}{2I_x} \left( \frac{H^2}{4} - \frac{h^2}{4} \right)$$

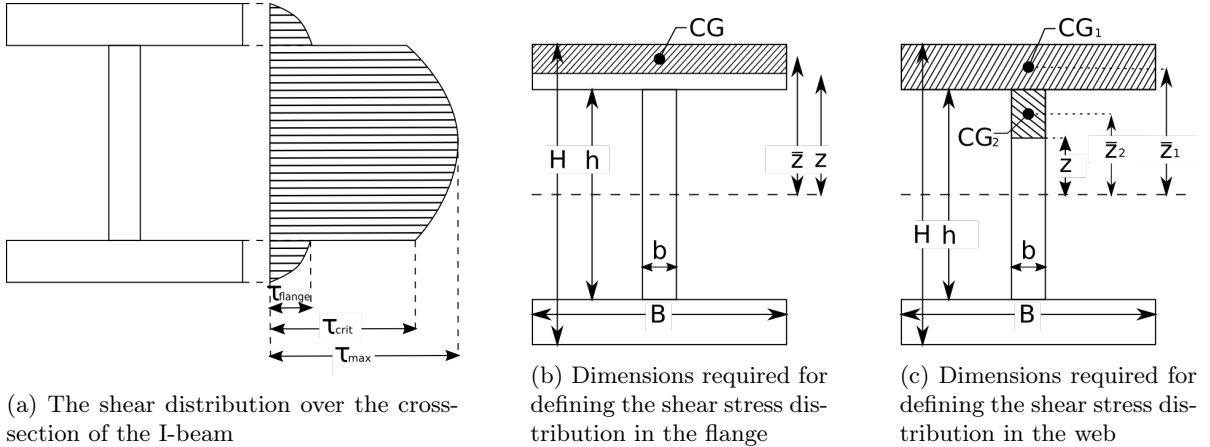


Figure A.2

The derivation for the shear distribution of the web is slightly different because the first moment of area of the web does also include the flange. The dimensions used for this derivation can be seen in Figure A.2c.

$$S_x = A_1 \cdot \bar{z}_1 + A_2 \cdot \bar{z}_2 \quad (\text{A.8})$$

$$A_1 = B \cdot \left( \frac{H}{2} - \frac{h}{2} \right) \quad (\text{A.9})$$

$$\bar{z}_1 = \frac{h}{2} + \frac{1}{2} \left( \frac{H}{2} - \frac{h}{2} \right) = \frac{H}{4} + \frac{h}{4} \quad (\text{A.10})$$

$$A_2 = b \cdot \left( \frac{h}{2} - z \right) \quad (\text{A.11})$$

$$\bar{z}_2 = z + \frac{1}{2} \left( \frac{h}{2} - z \right) = \frac{z}{2} + \frac{h}{4} \quad (\text{A.12})$$

$$S_x = B \cdot \left( \frac{H}{2} - \frac{h}{2} \right) \cdot \left( \frac{H}{4} + \frac{h}{4} \right) + b \cdot \left( \frac{h}{2} - z \right) \cdot \left( \frac{z}{2} + \frac{h}{4} \right) = \frac{B}{8} \cdot (H^2 - h^2) + \frac{b}{8} (h^2 - 4z^2) \quad (\text{A.13})$$

$$\tau_{web} = \frac{V_y}{I_x b} \left( \frac{B}{8} \cdot (H^2 - h^2) + \frac{b}{8} (h^2 - 4z^2) \right) = \frac{V_y}{I_x 8} \left( \frac{B}{b} \cdot (H^2 - h^2) + (h^2 - 4z^2) \right) \quad (\text{A.14})$$

The maximum shear stress occurs at  $z = 0$ . This results in the following maximum shear stress:

$$\tau_{max} = \frac{V_y}{I_x 8} \left( \frac{B}{b} \cdot (H^2 - h^2) + (h^2) \right) \quad (\text{A.15})$$

The shear stress in the connection, at the end of the shear web is the most critical. The stress has the following magnitude:

$$\tau_{critical} = \frac{V_y}{I_x 8} \left( \frac{B}{b} \cdot (H^2 - h^2) \right) \quad (\text{A.16})$$

# References

- [1] Susan L Bales. “Wave and wind data for seakeeping performance assessment”. In: *The International Towing Tank Conference, ITTC’83* (1983). URL: <https://repository.tudelft.nl/islandora/object/uuid%3A3f3406a-d72e-487f-b7c6-707d2e750eed>.
- [2] American Bureau of Shipping. “Guide for Building and Classing Yachts 2021 - Part 3, Hull Construction And Equipment”. In: (July 2021).
- [3] Bureau Veritas. “Hull in Aluminium Alloys, Design Principles, Construction and Survey - NR 561 DT R03 E”. In: (June 2021). URL: [https://erules.veristar.com/dy/data/bv/pdf/561-NR\\_2021-06.pdf](https://erules.veristar.com/dy/data/bv/pdf/561-NR_2021-06.pdf).
- [4] Bureau Veritas. “Rules for the Classification and the Certification of Yachts - NR 500 DT R02 E”. In: (June 2021). URL: [https://erules.veristar.com/dy/data/bv/pdf/500-NR\\_2021-06.pdf](https://erules.veristar.com/dy/data/bv/pdf/500-NR_2021-06.pdf).
- [5] H. S. Chan. “Prediction of motion and wave loads of twin-hull ships”. In: *Marine Structures* 6.1 (Jan. 1993), pp. 75–102. ISSN: 0951-8339. DOI: 10.1016/0951-8339(93)90010-Z.
- [6] G. R. Cowper. “The Shear Coefficient in Timoshenko’s Beam Theory”. In: *Journal of Applied Mechanics* 33.2 (June 1966), pp. 335–340. ISSN: 0021-8936. DOI: 10.1115/1.3625046. URL: <https://asmedigitalcollection.asme.org/appliedmechanics/article/33/2/335/386601/The-Shear-Coefficient-in-Timoshenko-s-Beam-Theory>.
- [7] DNV GL. “Recommended Practice DNV GL as Column-stabilised units”. In: (2015).
- [8] V Dubrovsky and A Lyakhovitsky. *Multihull ships*. 2001. ISBN: 0964431122.
- [9] O. M. Faltinsen. “Sea Loads on Ships and Offshore Structures”. In: *Ship Hydromechanics and Structures* (1990). URL: [https://books.google.com/books/about/Sea\\_Loads\\_on\\_Ships\\_and\\_Offshore\\_Structur.html?hl=nl&id=qZq4Rs2DZXoC](https://books.google.com/books/about/Sea_Loads_on_Ships_and_Offshore_Structur.html?hl=nl&id=qZq4Rs2DZXoC).
- [10] Stefano Ghelardi, Marco Gaiotti, and Cesare M. Rizzo. “On the shear lag effective breadth concept for composite hull structures”. In: *Ship and Offshore structures Volume 3* 10.3 (May 2014), pp. 272–289. ISSN: 17445302. DOI: 10.1080/17445302.2014.887172. URL: <https://www.tandfonline.com/doi/abs/10.1080/17445302.2014.887172>.
- [11] S. E. Heggelund, T. Moan, and S. Oma. “Determination of global design loads for large high-speed catamarans”. In: *Engineering for the Maritime Environment* 216.1 (Dec. 2005), pp. 79–94. ISSN: 20413084. DOI: 10.1243/147509002320382158. URL: <https://journals-sagepub-com.tudelft.idm.oclc.org/doi/10.1243/147509002320382158>.
- [12] I.G. Tigkas and A. Theodoulides. “On the effective breadth of plating”. In: *Sustainable Maritime Transportation and Exploitation of Sea Resources*. Ed. by Enrico Rizzuto and C. Guedes Soares. London : CRC Press, 2011. ISBN: 9780429098444.
- [13] Jørgen Juncher Jensen. *Load and global response of ships*. Amsterdam ; Elsevier, 2001. ISBN: 0080439535.
- [14] Fuat Kara. “Time domain prediction of seakeeping behaviour of catamarans”. In: *International Shipbuilding Progress* 62.3-4 (Jan. 2015), pp. 161–187. ISSN: 0020-868X. DOI: 10.3233/ISP-160120.
- [15] F.W. Lambert. *The theory and practical design of bunkers*. 1968. URL: <https://www.steel.org.au/resources/elibrary/library/the-theory-and-practical-design-of-bunkers-by-f-w-lambert/>.
- [16] NATO - STANAG 4194 - Standardized Wave and Wind Environments and Shipboard Reporting of Sea Conditions | *Engineering360*. Tech. rep. NATO, Apr. 1983.
- [17] Raymond J. Roark, Warren C. Young, and Robert Plunkett. “Formulas for Stress and Strain”. In: 1965. ISBN: 0070725411.

- [18] Debarata Sen and Amresh Negi. “Computation of wave induced motions and loads on catamaran hulls with forward speed”. In: *International Journal of Naval Architecture and Ocean Engineering* (Sept. 2016). ISSN: 20926782. DOI: 10.1016/J.IJNAOE.2016.08.005. URL: [https://www.researchgate.net/publication/308040345\\_Computation\\_of\\_wave-induced\\_motions\\_and\\_loads\\_on\\_catamaran\\_hulls\\_with\\_forward\\_speed](https://www.researchgate.net/publication/308040345_Computation_of_wave-induced_motions_and_loads_on_catamaran_hulls_with_forward_speed).
- [19] Ship structure committee. *Catamarans technological limits to size and appraisal of structural information and procedures*. Tech. rep. USA, 1971.
- [20] Craig B Smith. “Extreme Waves and Ship Design”. In: (2007). URL: <http://shipstructure.org/pdf/2007symp09.pdf>.
- [21] A.P. Van 't Veer. *Behaviour of catamarans in waves*. 1998. URL: <https://repository.tudelft.nl/islandora/object/uuid%5C%3Afc4c765a-3c7f-412d-9607-94fb9081ff36>.
- [22] Warren C Young et al. *Roark's Formulas for Stress and Strain*. 1976. ISBN: 007072542X.